Chapter 1

Introduction

1.1 Background

Thin-film transistor (TFT) liquid-crystal displays (LCD), widely used to support full-featured multimedia, go toward higher resolution and larger panel sizes. The display components are always active mode, while the CPU and the memory are in power down mode during the slack time. This makes the LCD backlight a major source of power dissipation [1]. Thus, reducing backlight power consumption is one of the primary ways to extend operating time in battery-operated electronic devices.

Reduction of power consumption through backlight control is one of the most important requirements for displays used in mobile applications. One way of achieving this is by sensing the ambient illumination conditions of the display. Under conditions of low ambient illumination the display brightness can be lowered saving power and reducing glare. Currently discrete photo diodes are used for most ambient light sensing systems.

However, normal environment illumination may contain over 3 orders of magnitude (60 dB or 10-bit) variation from the darkest to the brightest region. To cover such a wide range with linear photo detectors requires not only excessive output bandwidth but also high signal-to-noise ratio (SNR) of the sensor. This may impose the complexity and incidental power consumption on the system.

Figure 1-1 shows the structure of photodiode. To improve SNR, for practical applications, it is necessary to increase the size of the photo detectors to resolve small difference [2].

However, large size photodiode may cause additional power consumption at high illumination levels and not suit with working in the pixel.

Integration of light sensors reduces module complexity and location of the sensors close to the pixel array simplifies integration in products. There is an interest in integrating the sensors in the same TFT technology used to fabricate the display so that the overall complexity of the module can be reduced. Since the sensors are fabricated on the glass substrate using the same fabrication processes as conventional TFTs, fabrication costs can be saved.

1.2 Motivation

In this thesis, we explore a method to sense the light with small size devices which have the same fabrication processes as conventional a-Si:H TFTs. A non-conventional structure of a-Si:H TFT is proposed to achieve good photosensitivity in ON region for low illumination intensity, while keeping its size small by operation in OFF region for high intensity sensing.

1.3 Thesis Organization

After introduction of Chapter 1, the photo offset of device will be discussed in Chapter 2. Then the corresponding sensing circuit will be described in chapter 3. The error factors of the proposed method will be analyzed in Chapter 4. Finally, conclusions will be given in Chapter 5. The section organization of this thesis is listed below:

Chapter 1 Introduction

1.1 Background

1.2 Motivation

1.3 Thesis Organization

Chapter 2 Photo Effect on Device

2.1 The Different Structures of a-Si TFTs

2.2 Photo Effect of Front Light Illumination

2.3 Analysis of Sensitivity in ON and OFF regions

Chapter 3 Light Sensing Circuit

3.1 Conventional Light Sensing Circuit

3.2 Sensor Structure and Operation Principle

3.2.1 OFF Region Sensing Circuit (3T1C)

3.2.2 ON Region Sensing Circuit (4T2C)

3.3 Simulation

3.3.1 Simulation Method

3.3.2 Simulation Method Result

3.3.3 Discussion

3.4 Digitalization

Chapter 4 Error Factors

4.1 Uniformity

4.2 Temperature

4.3 Back Light

4.4 Staebler-Wronski Effect

4.4.1 Same Degradation Ratio of Photo current under FL Stress

4.4.2 Top Metal Shielding Ratio

4.4.3 Without Back Light Stress

4.4.4 With Back Light Stress

4.5 Discussion

Chapter 5 Conclusions

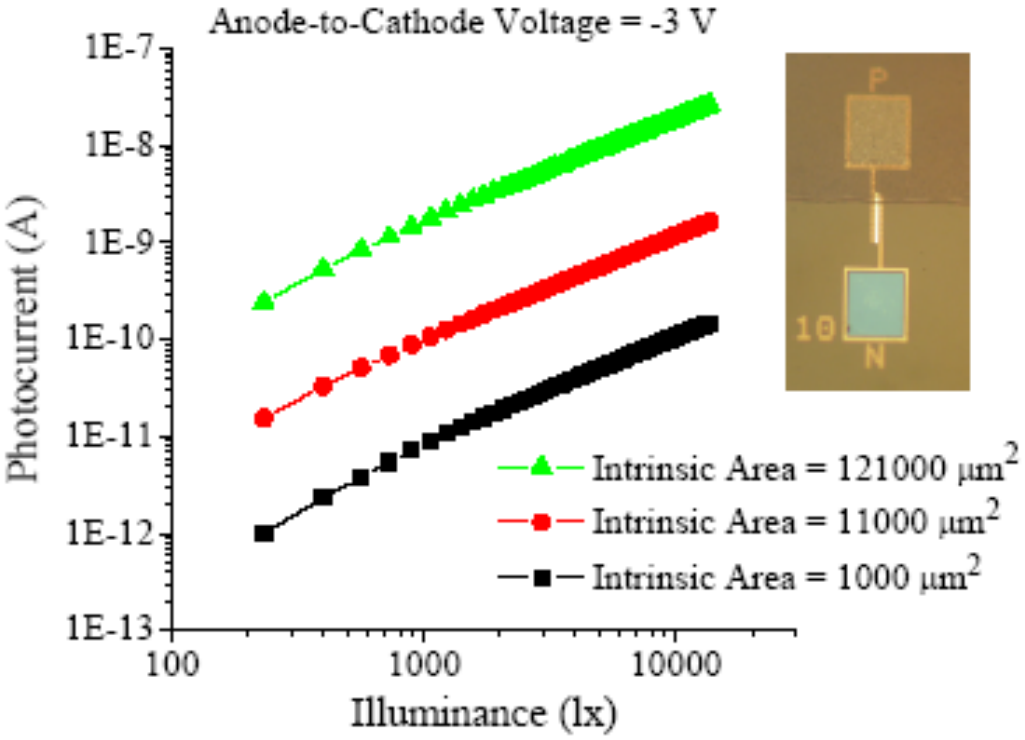

Fig. 1-1 The linearity between the illuminance and the photocurrent of lateral PIN photodiodes with area =1000/11000/121000 μm^2 (Ref. *Hyun-Sang Park et al.,SID' 08*)

Chapter 2

Photo Effect on Device

2.1 The Different Structures of a-Si TFTs

The a-Si:H TFTs used in this thesis are the conventional bottom-gate inverted staggered structure and fabricated on the glass substrates. The cross-section views of a-Si:H TFTs are shown in Figure 2-1(a). After the deposition and patterning of gate metal on the glass substrates, three layers, i.e., silicon nitride (SiNx, 3500 Å), a-Si:H, and n+ a-Si:H films, were successively deposited in a plasma enhanced chemical vapor deposition (PECVD) system. After making the source/drain electrodes, the n+ a-Si:H region with length (L) of 5 μm between the source/drain electrodes was etched off by a reactive ion etch. Then, a passivation layer was used to cap the channel region.

The device structure of a Gap-Gate photo-TFT is shown in Figure 2-1(b) [3]. Its structure differs from that of the conventional TFT in that its source contact is recessed from the gate electrode to form a highly-resistive Gap-Gate gap region. Figure 2-1(c) shows that structure of Dual-Gate TFT. The Dual-Gate TFT has almost the same structure as the conventional TFT, expect that Dual-Gate TFT has slit-gate electrodes (gate-A and gate-B in Figure 2-1(c)) [4]. Because the structure of these TFTs and conventional TFTs are similar, the Dual-Gate TFTs can be fabricated in the same process as the conventional TFTs, they can be successfully applied in active-matrix LCDs.

A detailed analysis and better understanding of the effect of illumination on the a-Si TFTs electrical performances are necessary before the device is applied to be

used as a photo-sensor. In our research, to increase SNR, we will select a structure by considering the characteristics of current low dark current (I_{D_dark}), high illumination current (I_{D_illum}), and high $R_{L/D}$ (I_{D_illum} / I_{D_dark}) [5].

2.2 Photo Effect of Front Light Illumination

Figure 2-2, figure 2-3, and figure 2-4 show the a-Si TFTs transfer characteristics in the dark as well as irradiated at six different levels of halogen lamp illumination from the front side. For the three TFT structures, namely, conventional-gate, Gap-Gate, and Dual-Gate, their current levels and photosensitivities are discussed.

The devices are bias in the ON, subthreshold, and OFF regimes, in the range of V_{gs}= -15 ~ +15V. We can observe the significant difference of the photosensitivity among these structures, as can be seen in figure 2-2, figure 2-3 and figure 2-4. Considering the possible threshold voltage shift of the TFT, subthreshold region is not suitable for practical use. Thus we will only focus on the ON and OFF regions.

Figure 2-2 shows that the drain current is almost independent of illumination intensity when the conventional-gate TFT operates in the ON region. In OFF region, we can see the photosensitivity is significantly higher than that in the ON-state.

Figure 2-3 shows that structures of Gap-Gate TFT. Since the Gap-Gate TFT is asymmetric, it has two kinds of operation. Figure 2-3(a) is the gate-near-drain one, and figure 2-3(b) is the gate-near-source one. For further discussion, we define the ratio of the TFT drain current under illumination (I_{D_illum}) to that in the dark (I_{D_dark}) as $R_{L/D} = I_{D\_illum} / I_{D\_dark}$. We can find that the $R_{L/D}$ of the gate-near-source one is not only larger than that in OFF region (Vgs = -10V) but also in ON region (Vgs = 10V). In aspect of application, the gate-near-source one has better photosensitivity to be the sensing device. From figure 2-3(b), we can see its $R_{L/D}$ can achieve to 4 orders both in

OFF region and ON region.

Figure 2-4 shows that structures of Dual-Gate TFT. The Dual-Gate TFT is also asymmetric, and can be alternatively operated. Figure 2-4 (a) and (c) are of the gate(A)-near-drain one , and figure 2-4 (b) and (d) are of the gate(A) -near-source one. They show that the photo sensitivity of the Dual-Gate with positive gate(B) voltage is similarly to that of the Gap-Gate one but lower. While the Dual-Gate with negative gate(B) voltage has photo sensitivity independent of gate (A) voltage.

Table 2-1 compares of the $R_{L/D}$ and current level in the dark of the conventional-gate, Gap-Gate, and Dual-Gate TFTs. Although the conventional-gate TFT has current level of ON-state 3 to 7 orders larger than the others, it has poorer $R_{L/D}$ in the ON-state. From the view point of photosensitivity, the high ON current of the conventional-gate TFT is not suitable for the light sensing application, but it is suitable for being used in the circuit of the readout part. The high illumination current and the low dark current lead to the dynamic range. In the aspects of the photo sensing sensitivity. For this reason, the Gap-Gate TFT is chosen to be the sensing device and only its behaviors are considered in the rest of this thesis.

2.3 Analysis of Sensitivity in ON and OFF regions

As mentioned above, only the Gap-Gate TFT will be discussed. Figure 2-5(a) shows the relationships between photo current in the ON region and illumination intensity for several bias conditions. It can be seen that the increasing rate of the photo current under high illumination intensity is much less than that under weak light. For other words, it has poorer photosensitivity when device is operated under higher illumination. Therefore, instead, we propose to use the device in OFF region. As shown in figure 2-5(b), the photo current keeps almost linearity increasing rate with

illumination.

To compare the current increasing rates in ON and OFF regions, we normalized the currents in figure 2-5 to their corresponding maximum currents. The normalized result, in ON and OFF regions at V_D=10V are plotted together in figure 2-6(a). We further differentiate the curves of figure 2-6(a). To obtain the relative changing rate of photo current, namely, the relative photosensitivity versus illumination intensity and plot in figure 2-6(b). An intersection point at about 18860 lux is needed at the first sight. It means that sensing device operated in ON region has better relative photosensitivity under 18860 lux illumination, while OFF region offers better relative photosensitivity above 18860 lux. Consequently, we propose to operate the sensing device in ON region for weak illumination. Even very weak illumination, ON region operation can provide the ON current about 2 orders higher than OFF current. The higher current signal can reduce the effect of noise and be read easily. On the other hand, the OFF current is used for high illumination sensing to achieve better sensitivity with moderate current level.

In such a case, we can design the sensing circuits for both the ON and OFF modes. By combining benefits of the two modes, the low current operation can be avoid to waive the effect of noise, and the sensitivity can be kept high. Thus, the target of wide dynamic range sensing can be achieved. The proposed sensing circuits will be described in Chapter 3 in more detail.

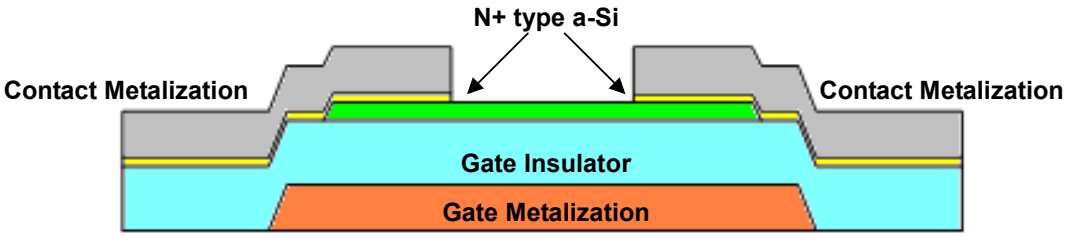

Fig. 2-1 (a) The cross-section views of Conventional-Gate a-Si TFTs structure

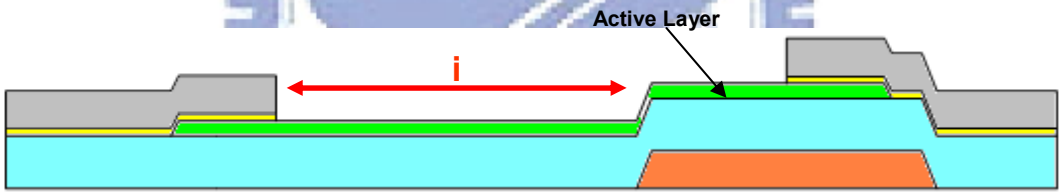

Fig. 2-1 (b) The cross-section views of Gap-Gate a-Si TFTs structure

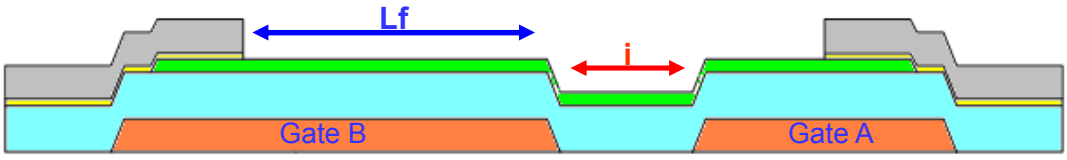

Fig. 2-1 (c) The cross-section views of Dual-Gate a-Si TFTs structure

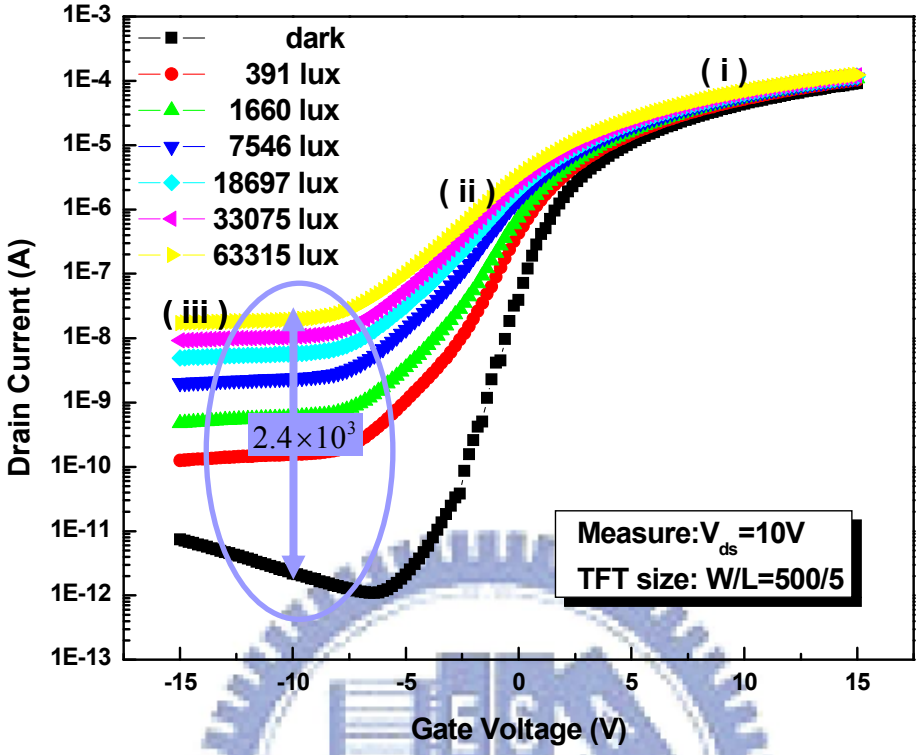

Fig. 2-2 Conventional gate TFT transfer characteristics in the dark and under illumination at V_{ds}=10V including regions (i) ON (ii) subthreshold (iii) OFF

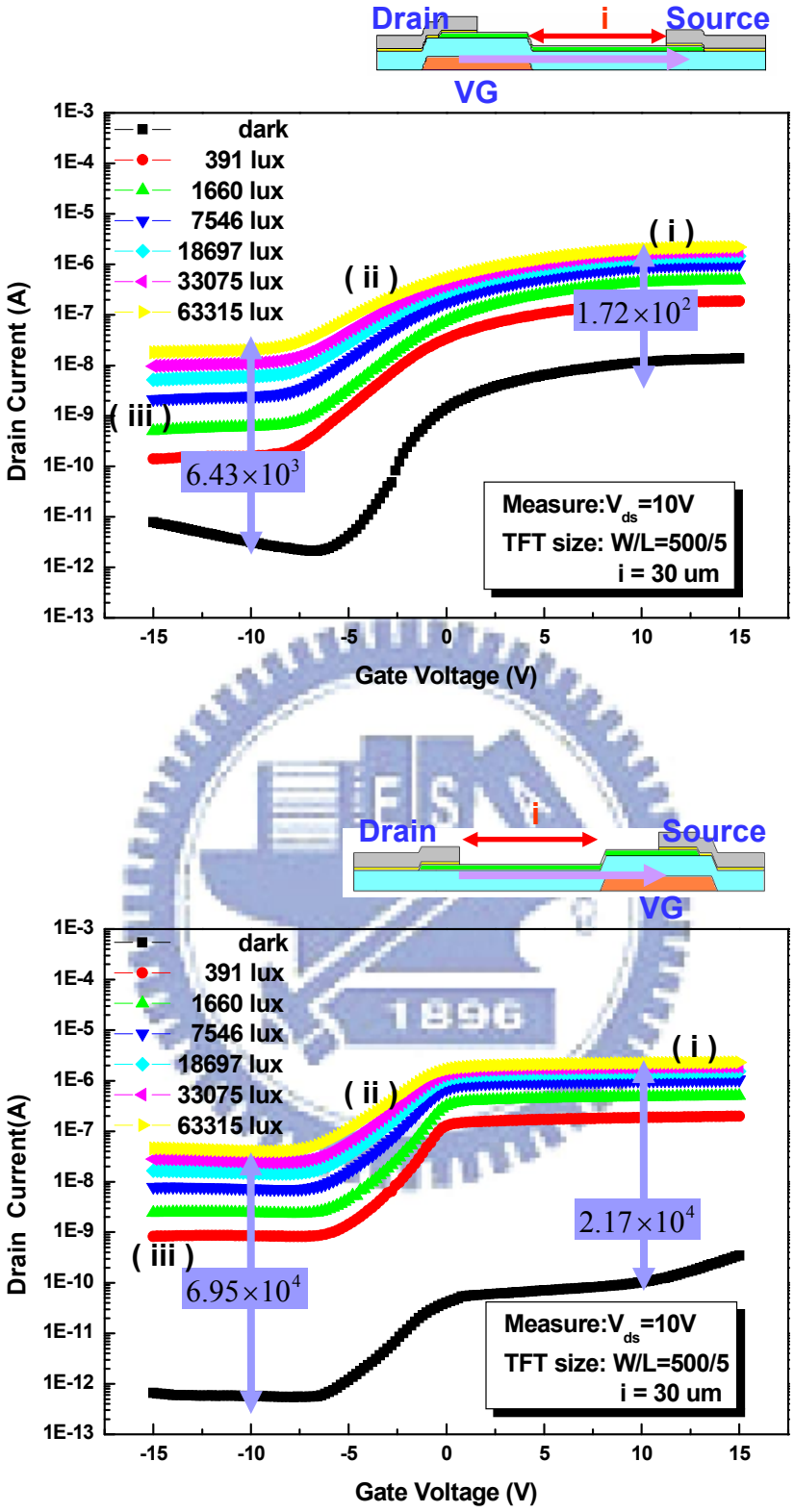

Fig. 2-3 (a) and (b) Gap-Gate TFT transfer characteristics in the dark and under illumination at V_{ds}=10V including regions (i) ON (ii) subthreshold (iii) OFF

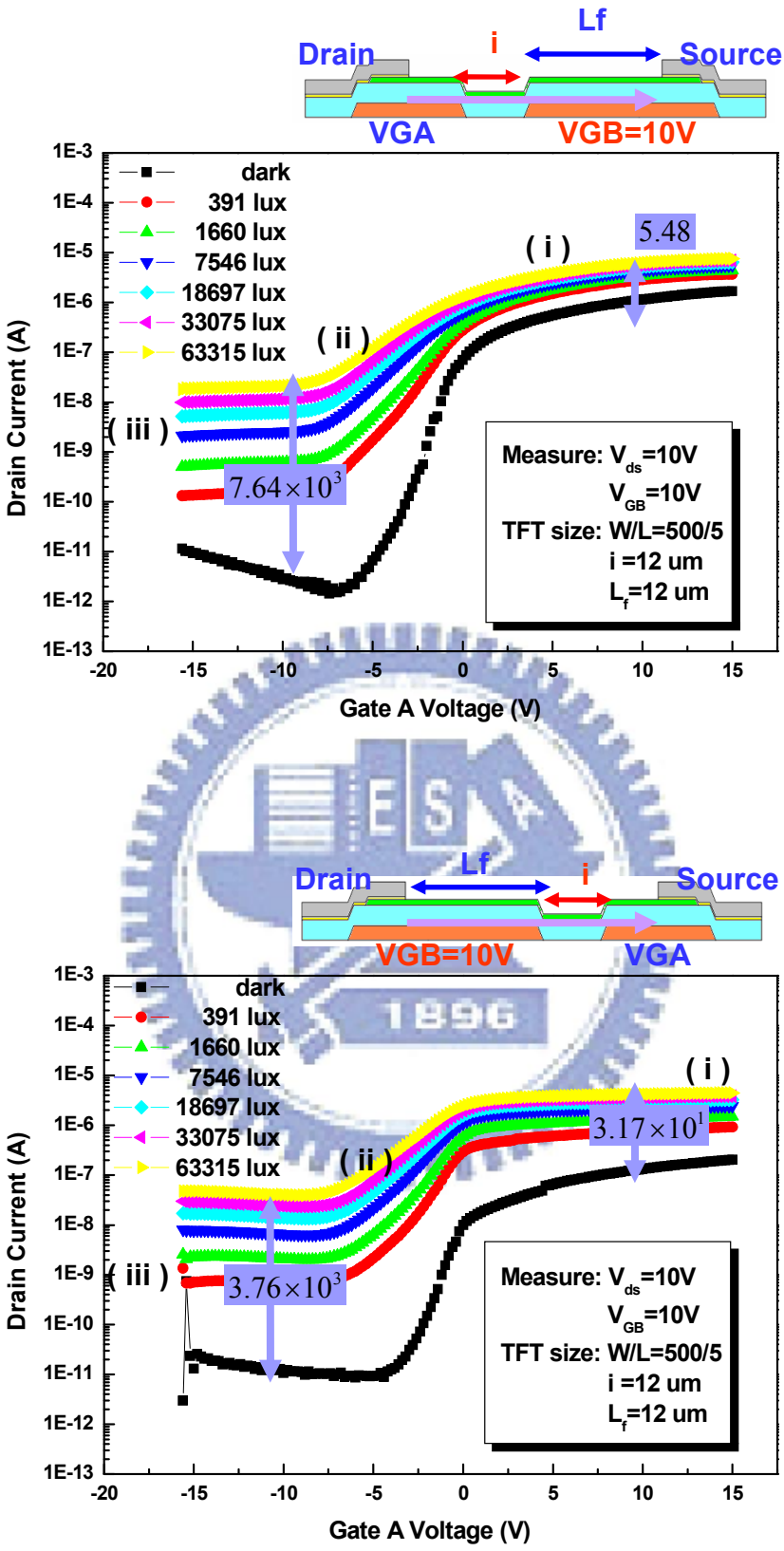

Fig. 2-4 (a) and (b) Dual-Gate TFT transfer characteristics in the dark and under illumination at V_{ds}=10V and V_{GB} =10V including regions (i) ON (ii) subthreshold (iii) OFF

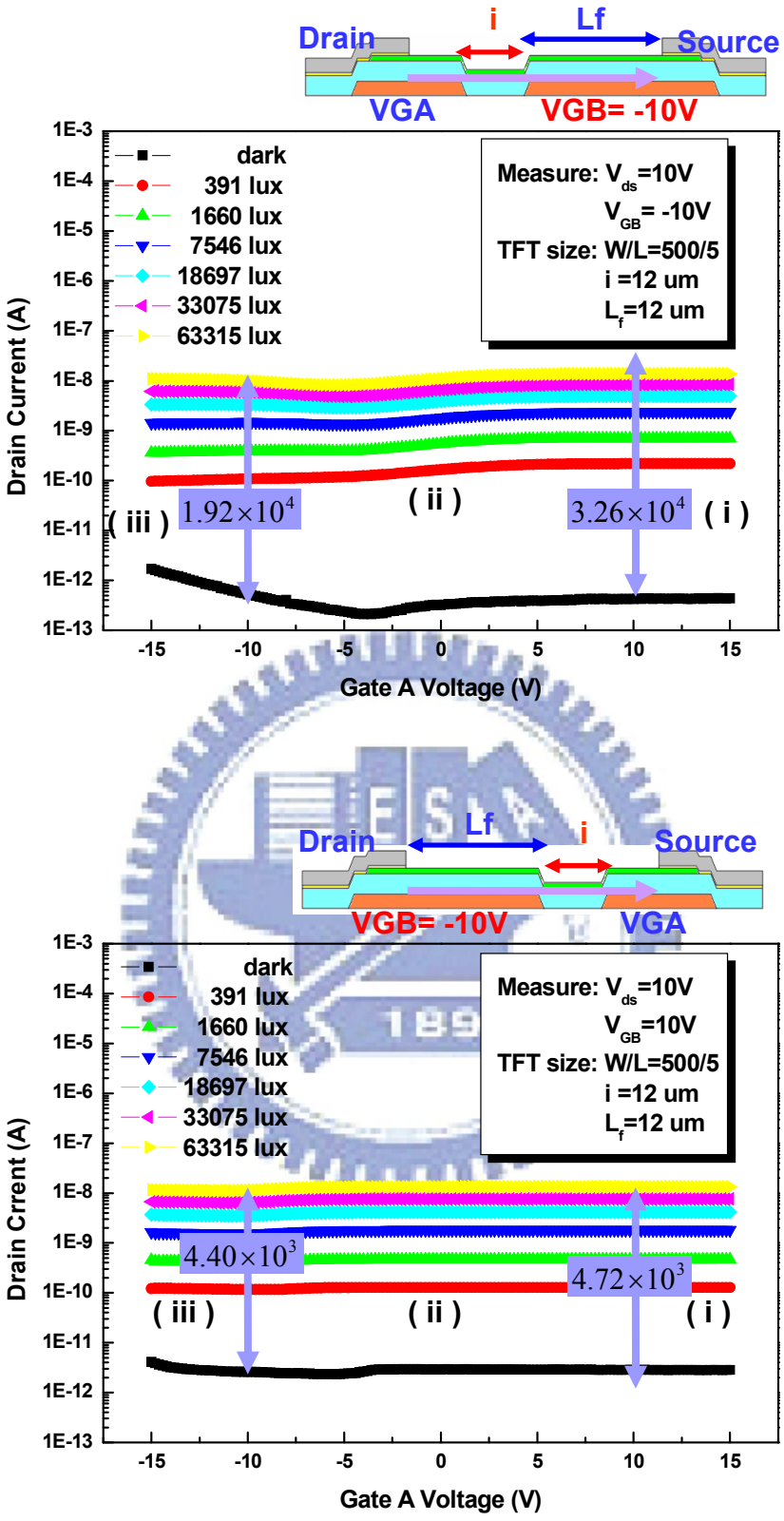

Fig. 2-4 (c) and (d) Dual-Gate TFT transfer characteristics in the dark and under illumination at V_{ds}=10V and V_{GB} = -10V including regions (i) ON (ii) subthreshold (iii) OFF

.

Sensing Device	Conventional		Source Gate		Dual Gate (VGB>0)		Dual Gate (VGB<0)	
Vgate	*ON*	*OFF*	*ON*	*OFF*	*ON*	*OFF*	*ON*	*OFF*
Dark current level I(dark)	10^{-4} A High	10^{-11} A Low	10^{-10} A Low	10^{-12} A Low	10^{-7} A Med	10^{-11} A Low	10^{-11} A Low	10^{-11} A Low
Device Sensitivity I(Illumin)/ I(dark)	$1x10^{0}$ Low	$2x10^{3}$ Med	$2x10^{4}$ High	$7x10^{4}$ High	$3x10^{2}$ Med	$4x10^{3}$ Med	$4x10^{3}$ Med	$5x10^{3}$ Med

Selection guidelines :
1. Sensitivity to light → higher sensitivity
2. Easy to be readout → higher current level

Tab. 2-1 The comparison of the $R_{L/D}$ under illumination and in the dark and the current level is shown in its inset among conventional-gate, gap-gate, and dual-gate TFT.

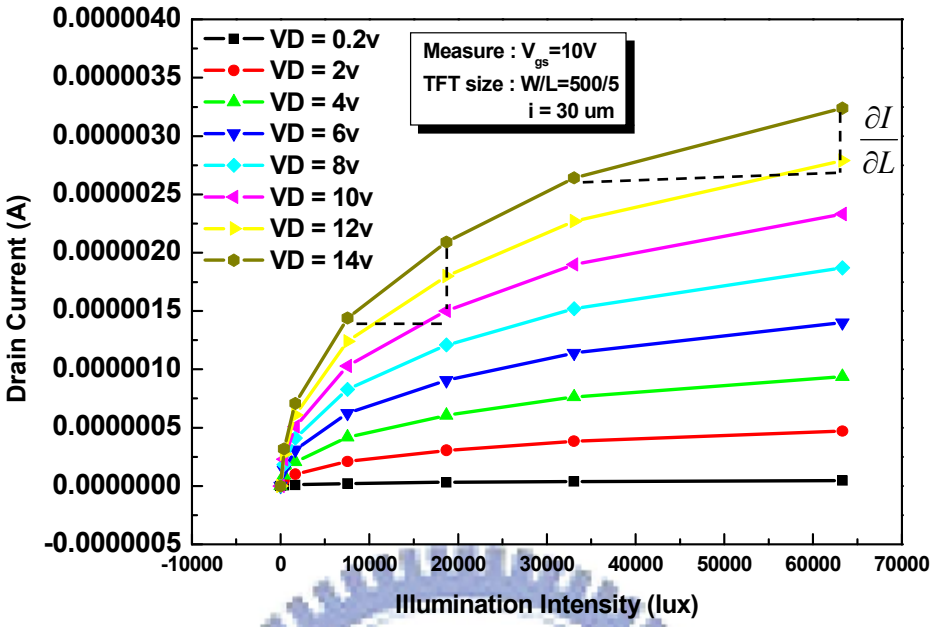

(a)

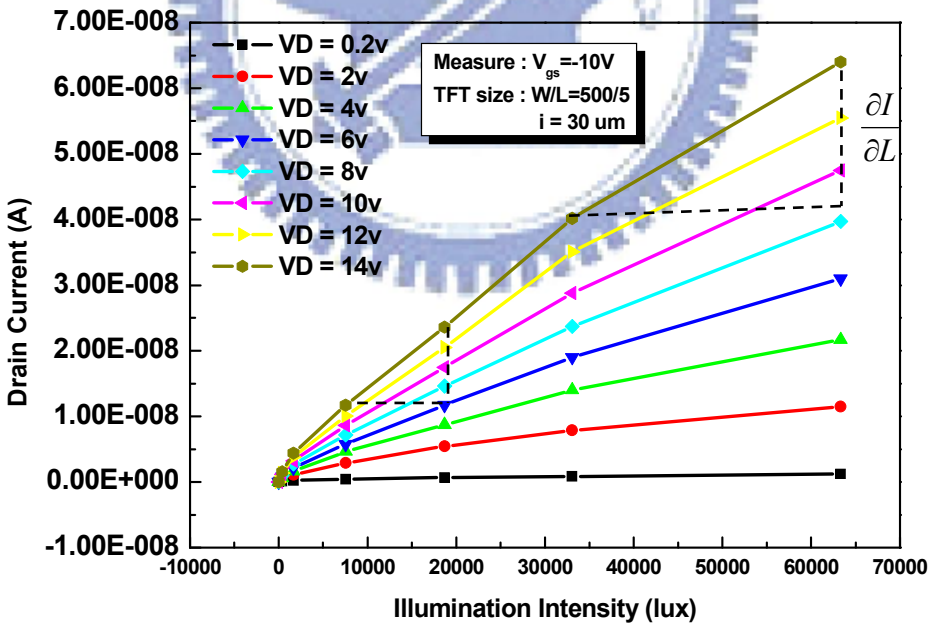

(b)

Fig. 2-5 The relationships between photo current and illumination intensity of Gap-Gate TFTs for several bias conditions in (a) the ON region and (b) OFF region, respectively.

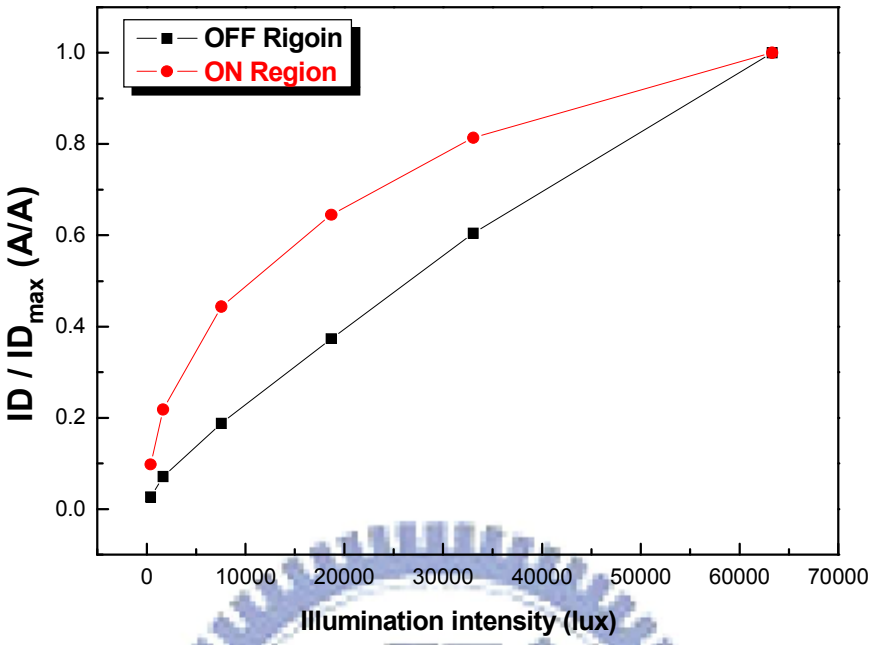

(a)

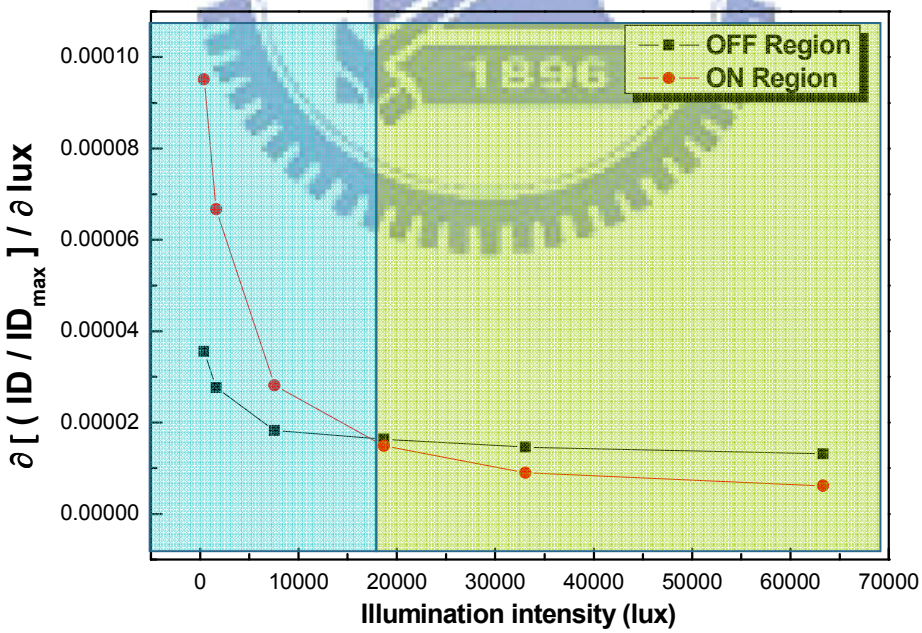

(b)

Fig. 2-6 show the comparison of the relative photo sensitivity between ON and OFF region.(a) after normalized , (b) after differentiation.

Chapter 3

Light-Sensing Circuit

3.1 Conventional Light Sensing Circuit

In conventional design, we use 1T1C to compose a sensing circuit which is showed in figure 3-1. The operating principles can be described as two periods shown in the timing diagram. In the charge period (1), when gate signal becomes “high”, T1 TFT is turned on. Thereby, the input voltage (V_{in}) “high” is stored in C_s and the voltage of node A (V_A) is charged to “V_{in_high}”. In the discharge period (2), the gate voltage of T1 is applied so that T1 is operating in the OFF region while sensing operation. At the same time, V_{in} becomes “low”. The photo leakage current drained away through the T1. The V_A is discharged by the photo leakage current of T1.

Because of the photo leakage current may also drain away through the readout path, we need to minimize this loading effect. There are several ways to achieve this purpose, and the most common method is using an operational amplifier (OP-Amp) [6- 7]. However, an OP-Amp using a-Si TFTs needs many transistors, which occupy too large area and increase power. Hence, we added a TFT (T2) to be a source follower readout part as shown in figure 3-2 [8-9]. A 2T1C light-sensing circuit and its timing sequence have been proposed [10].

The proposed 2T1C sensor has been fabricated on the glass substrate using a-Si technology for verification of light-sensing operation as shown in figure 3-3. Since the photo transistor of conventional circuit is designed as conventional TFT, we can sense front light. The output voltage of the proposed circuit is measured by oscilloscope during discharge period under illumination and in the dark. The output

waveforms are shown in figure 3-4 (a) and (b). The discharging rate of V_{out} which is due to photo leakage can be expressed as dV/dt. Consequently, the slopes (dV/dt) of the waveforms can reflect the drain current under illumination and in the dark, so that the illumination intensity can be sensed. Similarly, the conventional circuit also needs extra control bus to operate the photo transistor in proper region. Thus, considering the incorporation of our circuit design into the pixel, we will try to use the existing buses in the TFT-LCD pixel array but avoid adding new buses.

3.2 Sensor Structure and Operation Principle

After the discussions about illumination effect of Gap-Gate TFTs in chapter 2, we try to operate the device in the OFF and ON region under various ambient light circumstances. Because the drain current of TFT varies in a large range according to the illumination intensity, we proposed two circuits to sense the drain current under high and low illumination.

The proposed circuits are based on Gap-Gate TFTs characteristics to various sensing capability with photo transistors operated different regions. The system composed of 4T2C for ON region operation and 3T1C for OFF region in the sensing circuits. The sensing circuit for OFF region is shown in figure 3-5(a). The other one for ON region sensing circuit is shown in figure 3-6(a). For both circuits, the power and control buses are compatible with there in a TFTLCD panel. Next, we explain their operation respectably.

3.2.1 OFF Region Sensing Circuit (3T1C)

Figure 3-5 (a) and (b) show the schematic of the proposed 3T1C light-sensing circuit and its timing sequence, respectively. The proposed circuit consists of a

storage capacitor (C_S) and a photo (Gap-Gate) TFT, which channel width is 15 μm and length is 5 μm, as the sensing device.

The operating can be described as two periods shown in the timing diagram. In the charge period (1), scan line 1 becomes “high”, and thus photo TFT is turned on. Thereby, the voltage of node A (V_A) is charged to the input voltage (V_{com}) and stored in C_s. In the discharge period (2), the gate voltage of photo TFT is switched down so that photo TFT goes to the OFF region while sensing operation. At the same time, V_A goes “high” owing to the coupling from Cs. The photo leakage current, which is determined by the intensity of the ambient light, will be drained away through the photo TFT. And the V_A, which is held by C_s, is discharged by the photo leakage current of photo TFT in the slope corresponding to the light intensity.

3.2.2 ON Region Sensing Circuit (4T2C)

The other sensing circuit for ON region operation is shown in figure 3-6(a). In comparison with previous sensing part, it has a reset TFT and a design at couple capacitor (Cc). This circuit can offer higher current even signal under low illumination intensity.

The operating can be separated into two periods shown in the timing diagram. In the charge period (1), scan line 1 signal goes “high”, and thus reset TFT is turned on. Thereby, the input voltage (V_{com}) is passed through the reset TFT stored at node A (V_A) by Cs. In the discharge period (2), the gate voltage of photo TFT is set to ON by scan line 2 so that photo TFT is operating in the ON region while sensing operation. At the same time, V_A is coupling to “high”. The photo current, which is determined by the intensity of the ambient light, drained away through the photo TFT. And the V_A, held by C_s, is discharged by the photo current of photo TFT.

3.3 Simulation

For proposed light-sensing circuits as mentioned in the section 3.2, we necessary to simulate the behaviors of our light sensor before practical usage.

3.3.1 Simulated Method

In the RPI models of TFT, there is no photo current model for SPICE simulation [11], so we can not simulate the photo current under different illumination directly. We have to modify the simulation method according to illuminated characteristics of device. Figure 3-7 shows the illumination dependence of I_D-V_D characteristics curve; the drain current increased while the illumination intensity enhanced. We selected the approximately linear region of the I_D-V_D curve to fit the formula, which can be expressed as

$$I_D = I_0(L) + A_0(L) \cdot V_D \quad , \tag{2}$$

where $I_0(L)$ and $A_0(L)$ are respectively intercept and slope, which are both illumination dependence. Therefore, we use the different current sources and resistances in parallel to represent the different photo leakage currents of TFT. Table 3-1 and table 3-2 list the values of $I_0(L)$ and $R_0 = 1/A_0(L)$ at V_{gs}= -10V and 10V with the illumination intensity variation. When the illumination intensity changes, the value of $I_0(L)$ and R_0 change with it.

3.3.2 Simulated Results

Firstly, we focus on the readout part as shown in figure 3-5(a) and 3-6(a) and a switch TFT for multiplexing the readout signal from array to the readout path.

The ideal transfer characteristic of the switch source follower can be expressed as

$$V_{out} = V_{in} - V_{th}. \quad (1)$$

Figure 3-8 (a) and (b) show the simulation wave form of output signal when the input triangular signal is 5V to 14V. We can see the output waveform can work when the input frequency is 60kHz, which is compatible to the panel's operation frequency.

Next, we focus on the sensing device. Figure 3-9 shows the SPICE simulation results of TFT (W/L=500um/5um), for which we added a current source $I_0(L)$ and a resistance R_0 parallel to simulate the photo current as shown in its inset. In this figure, we can see the results already can represent the photo current can be simulated. Figure 3-10(a), figure 3-10(b), and figure 3-10(c) show the modified light-sensing circuits model for simulation and its time diagram. We can simulate the situations of TFT under various illumination conditions by this model. The simulation results are shown in the figure 3-11 (a) and (b). We can see in this figure, as expected, the output voltage (V_{out}) is discharged by the photo current of photo TFT. The larger the illumination intensity, the faster the discharge rate are.

3.3.3 Discussion

As the figure 3-11 (a) and (b) shown, we can see the response time is around 15 micro seconds in the simulated results as expected. We take further steps to compare the accuracy of the simulated results between ON region and OFF region. Figure 3-12 shows output voltage after 16us of discharge with respect to illumination intensity.

Figure 3-12(a) shows illumination dependence of circuit Vout of the sensing circuits. We defined the relative error with illumination as α = |dL/dVout|/L =|dL/L|/dVout. It means the relative error in lux arisen by a unit noise voltage. The

relationships between dynamic range and illumination intensity for propose system is shown in figure 3-12(b). With proper design, the overall error can be minimized to 1% per 1V of noise in V_{out}. These results reveal the circuits system we proposed can make best of the different photosensitivity characteristics of the TFT in ON and OFF regions to have the optimal performance.

Figure 3-13 (a) and (b) shows the layout configuration of our light-sensing circuits. Because the fabricated sample is not ready for practical measurement, the light-sensing operation and the output characteristic will verify in the future.

3.4 Digitization

In order to restrain the interference of noise and avoid the error due to V_{th} shift of source follower, a high accuracy ADC has been proposed. The digitization circuit is shown in figure 3-14(a), which consists of two comparators, a "AND" logic gate and a counter. Two reference voltages V_{ref_1} and V_{ref_2} are used to compare with V_{out}, we can adjust the range of V_{out} with different signals "V_{ref_1}" and "V_{ref_2}". If $V_{out} > V_{ref\_1} > V_{ref\_2}$ or $V_{ref\_1} > V_{ref\_2} > V_{out}$, the output of logic gate C is always "0", as shown in figure 3-14(b). Only when $V_{ref\_1} > V_{out} > V_{ref\_2}$, the output of logic gate C will be the clock numbers of CLK. Therefore, we can discriminate the slopes of V_{out} between different illumination intensities by counting the clock numbers. Moreover, in order to improve the resolution of the ADC, we can increase the speed of the CLK.

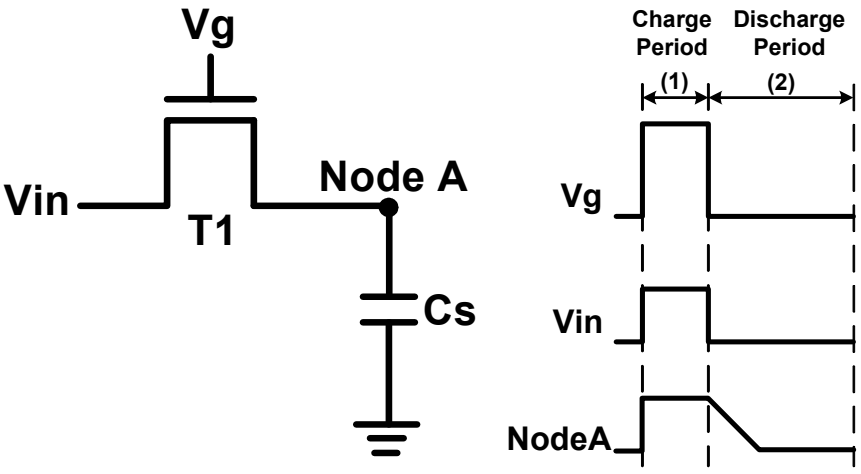

Fig. 3-1 Original light sensing circuit design

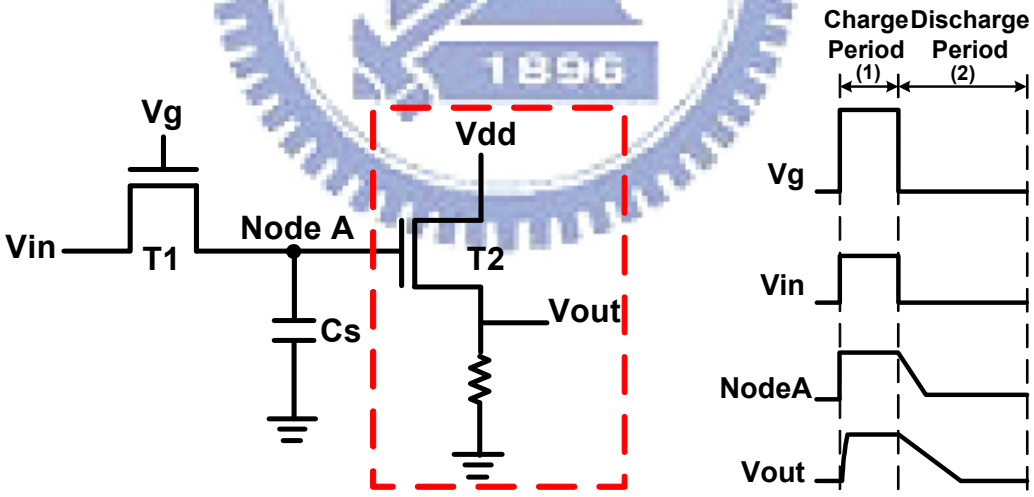

Fig. 3-2 Source follower as the readout part of sensor

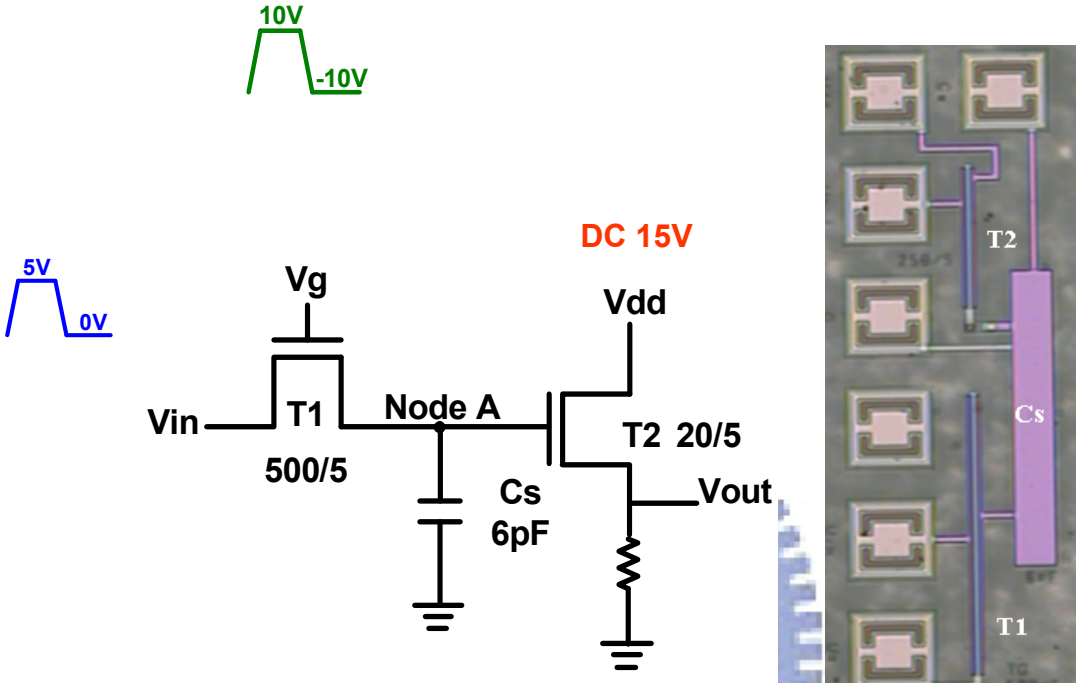

Fig. 3-3 Photograph of the fabricated 2T1C light-sensing circuit

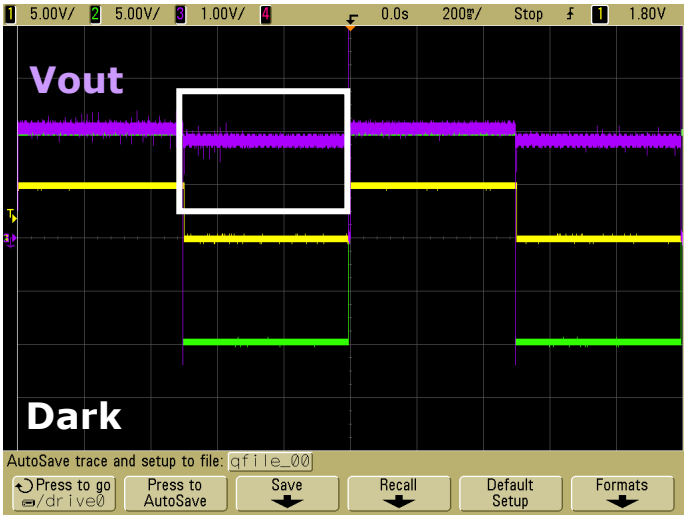

(a)

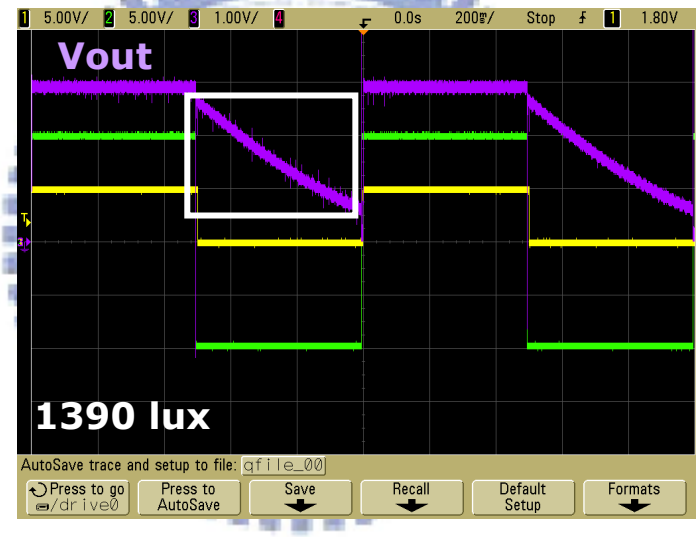

(b)

Fig. 3-4 Experiment result of light sensing circuit

(a) in the dark (b) under illumination

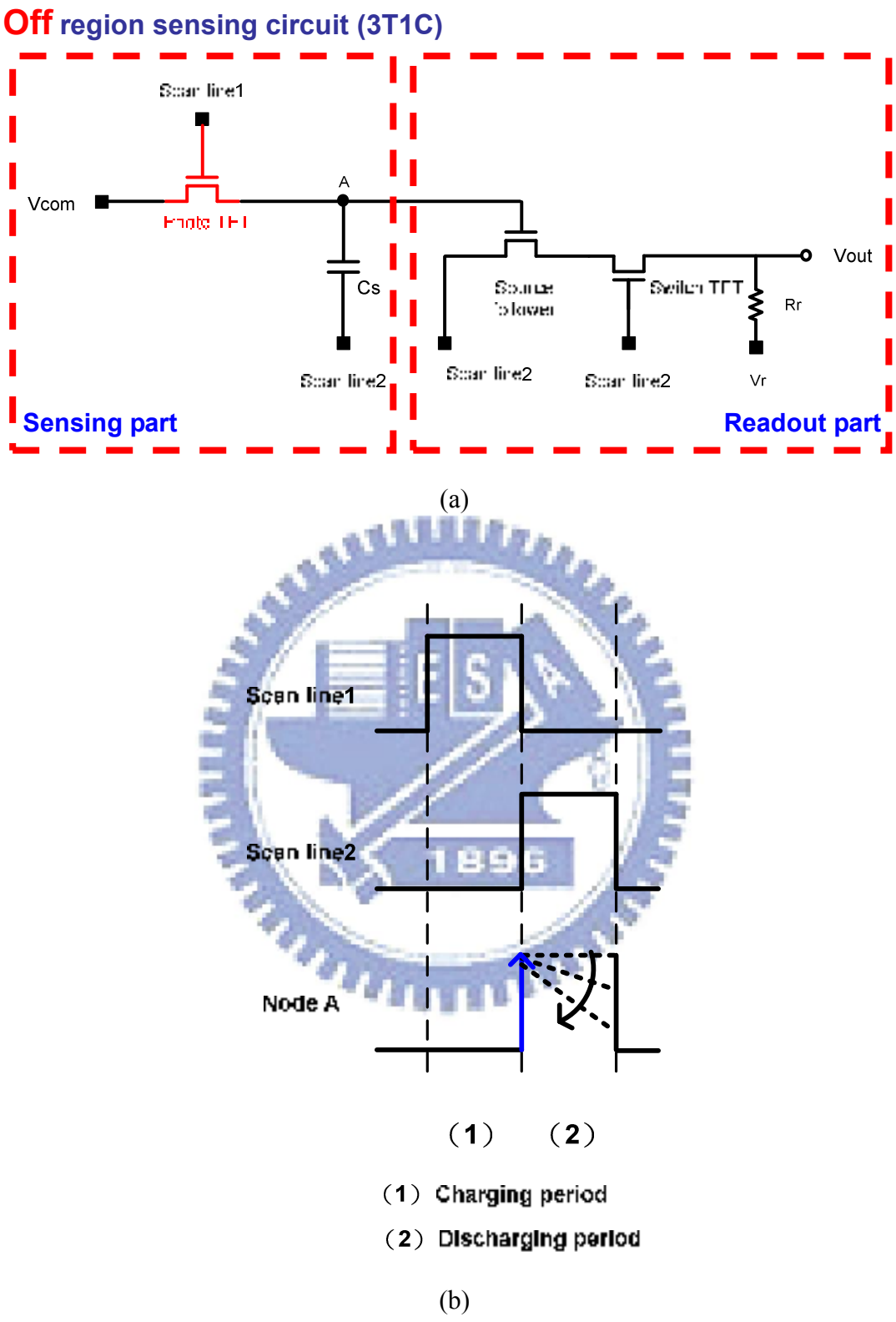

Fig. 3-5 (a) Schematic of proposed 3T1C light-sensing circuit and (b) timing sequence

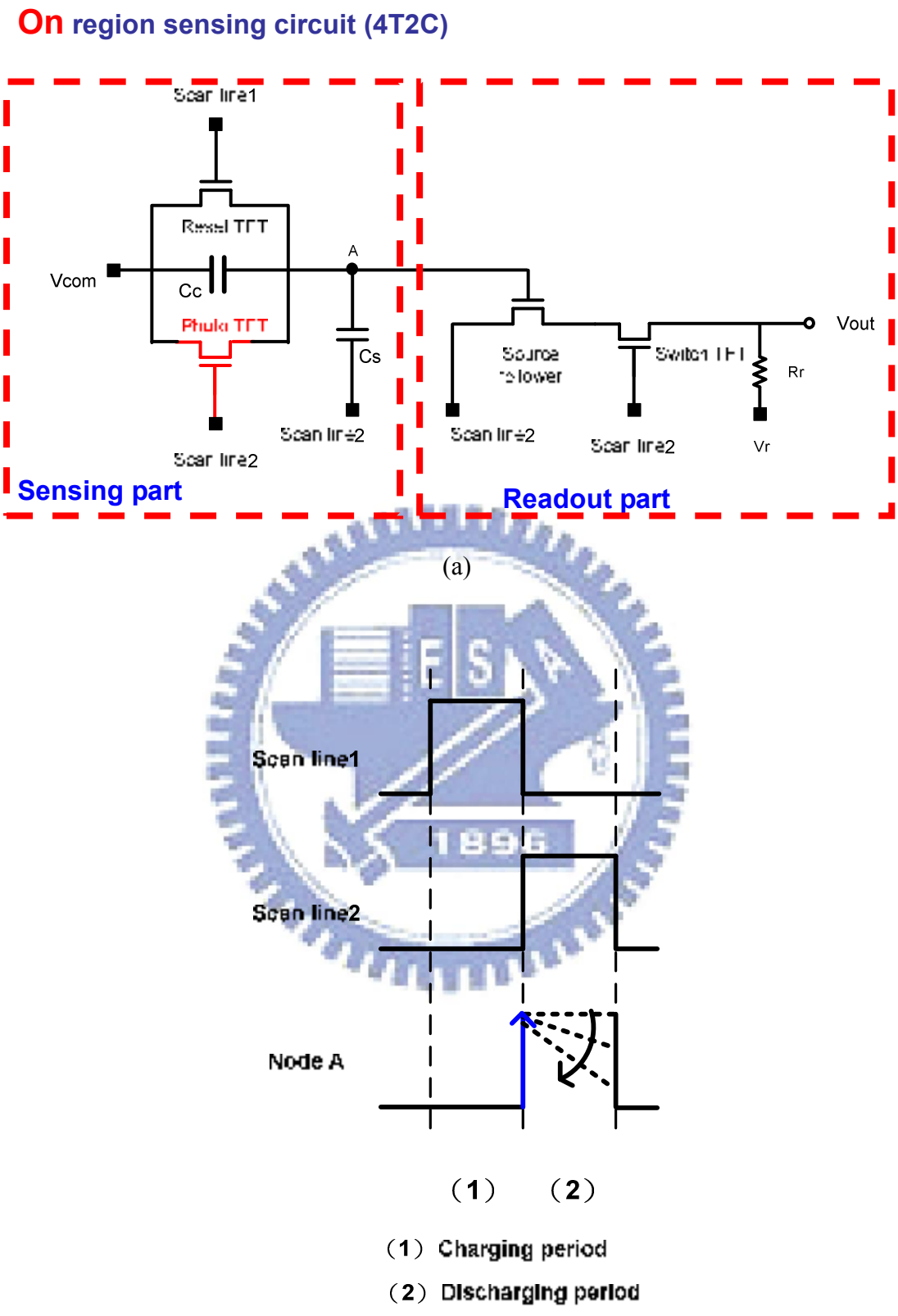

Fig. 3-6 (a) Schematic of proposed 4T2C light-sensing circuit and (b) timing sequence

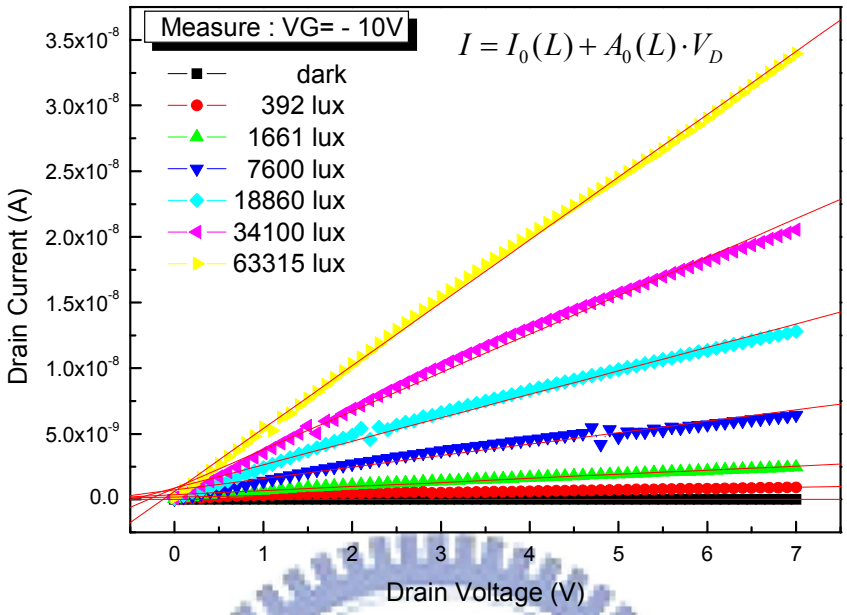

(a)

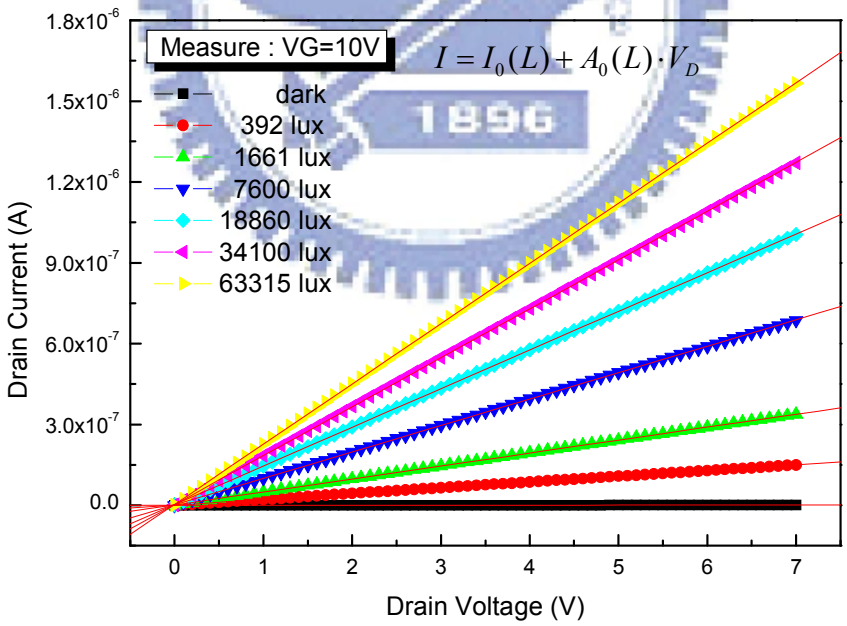

(b)

Fig. 3-7 Illumination dependence of I_D-V_D characteristic and its fitting formula in (a) OFF region and (b) ON region.

Table 3-1 $I_0(L)$ and $R_0 = 1/A_0(L)$ at V_g= -10V with the illumination intensity variation

Brightness	I0(L) [A]	R=1/A(L) [Ω]
Dark	**-1.65E-13**	**1.50E+13**
392lx	**1.96E-10**	**9.36E+9**
1660lx	**3.72E-10**	**3.22E+9**
7547lx	**7.35E-10**	**1.15E+9**
18698lx	**8.61E-10**	**5.59E+8**
33075lx	**8.71E-10**	**3.41E+8**
63315lx	**6.28E-10**	**2.09E+8**

Table 3-2 $I_0(L)$ and $R_0 = 1/A_0(L)$ at V_g= 10V with the illumination intensity variation

Brightness	I0(L) [A]	R=1/A(L) [Ω]
Dark	**-9.50E-12**	**4.83E+10**
392lx	**7.41E-10**	**4.32E+7**
1660lx	**1.05E-9**	**1.94E+7**
7547lx	**2.10E-9**	**9.64E+6**
18698lx	**2.67E-9**	**6.64E+6**
33075lx	**2.65E-9**	**5.26E+6**
63315lx	**2.48E-9**	**4.28E+6**

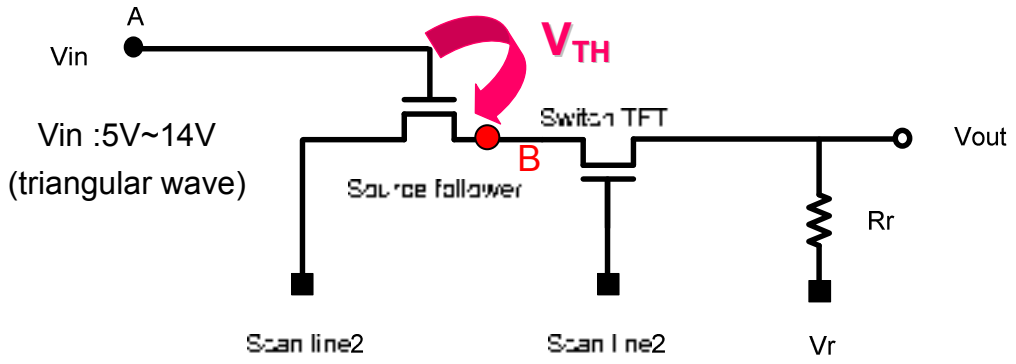

(a)

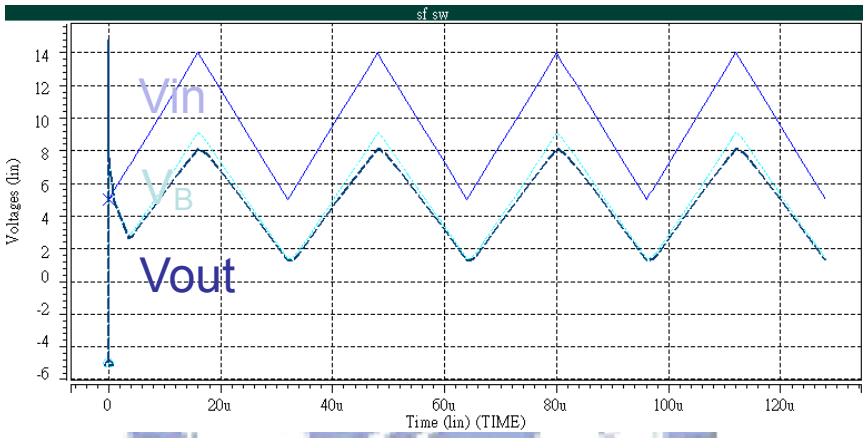

(b)

Fig. 3-8 (a) Schematic of conventional source follower (b) Wave form of the output signal when the input triangular signal is 5V to 14V

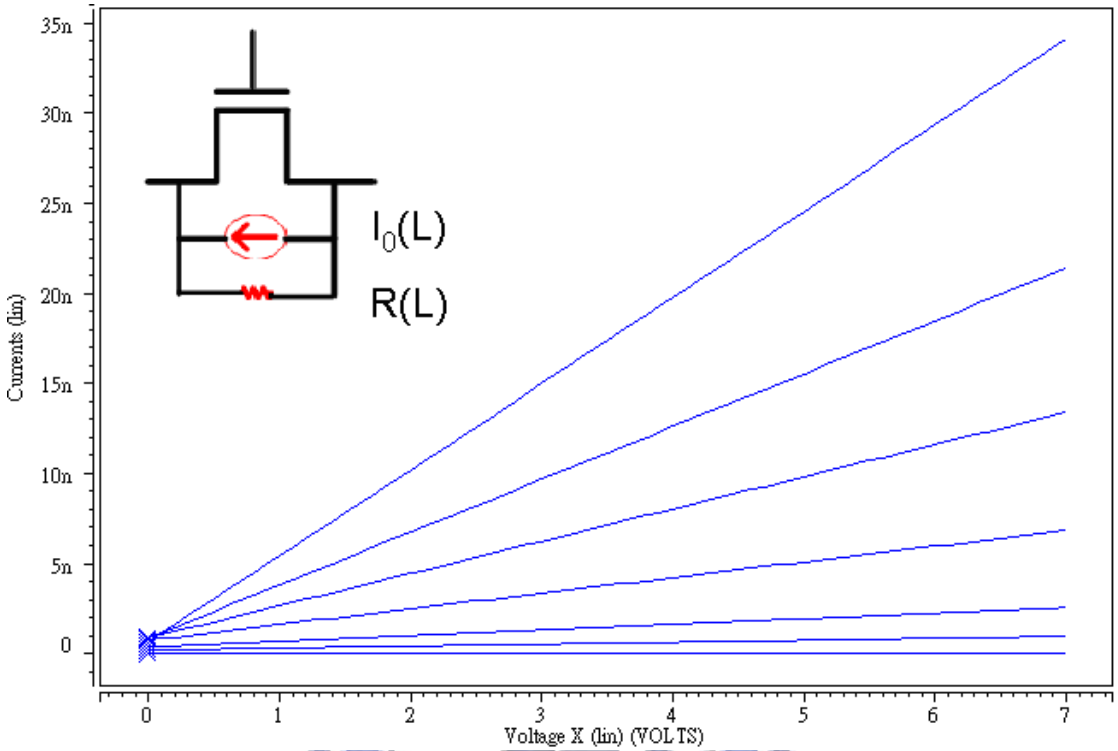

(a)

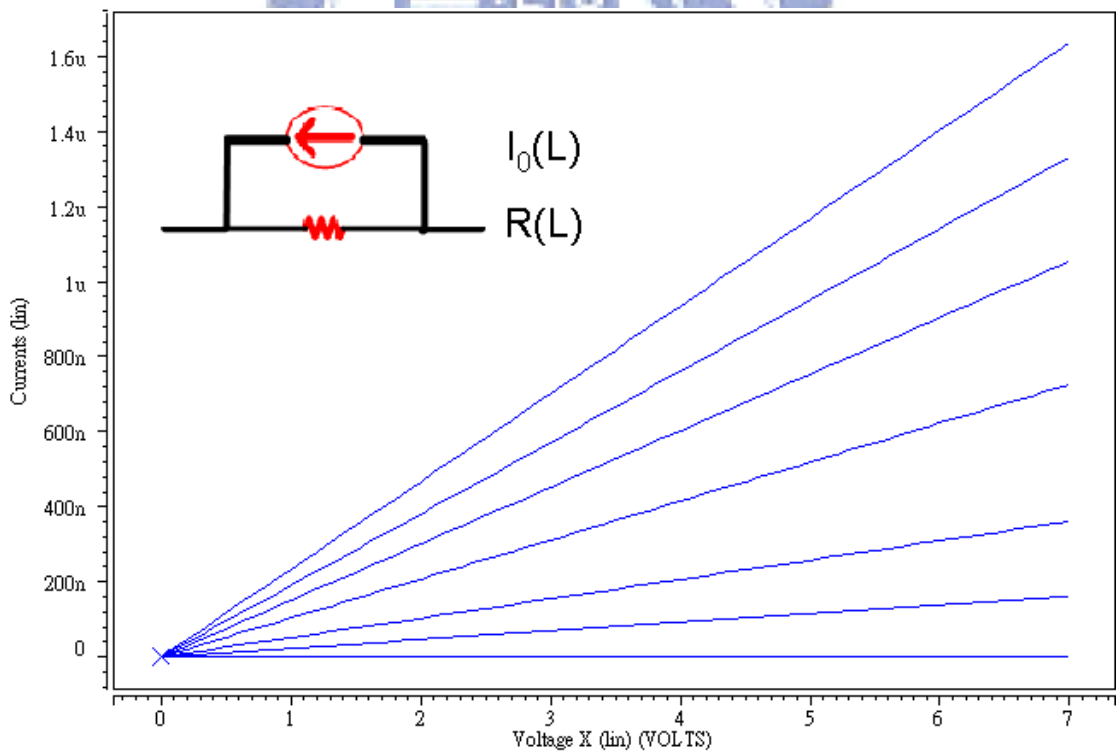

(b)

Fig. 3-9 SPICE simulation results of TFT (W/L=20um/5um) (a) OFF region sensing, (b) ON region sensing.

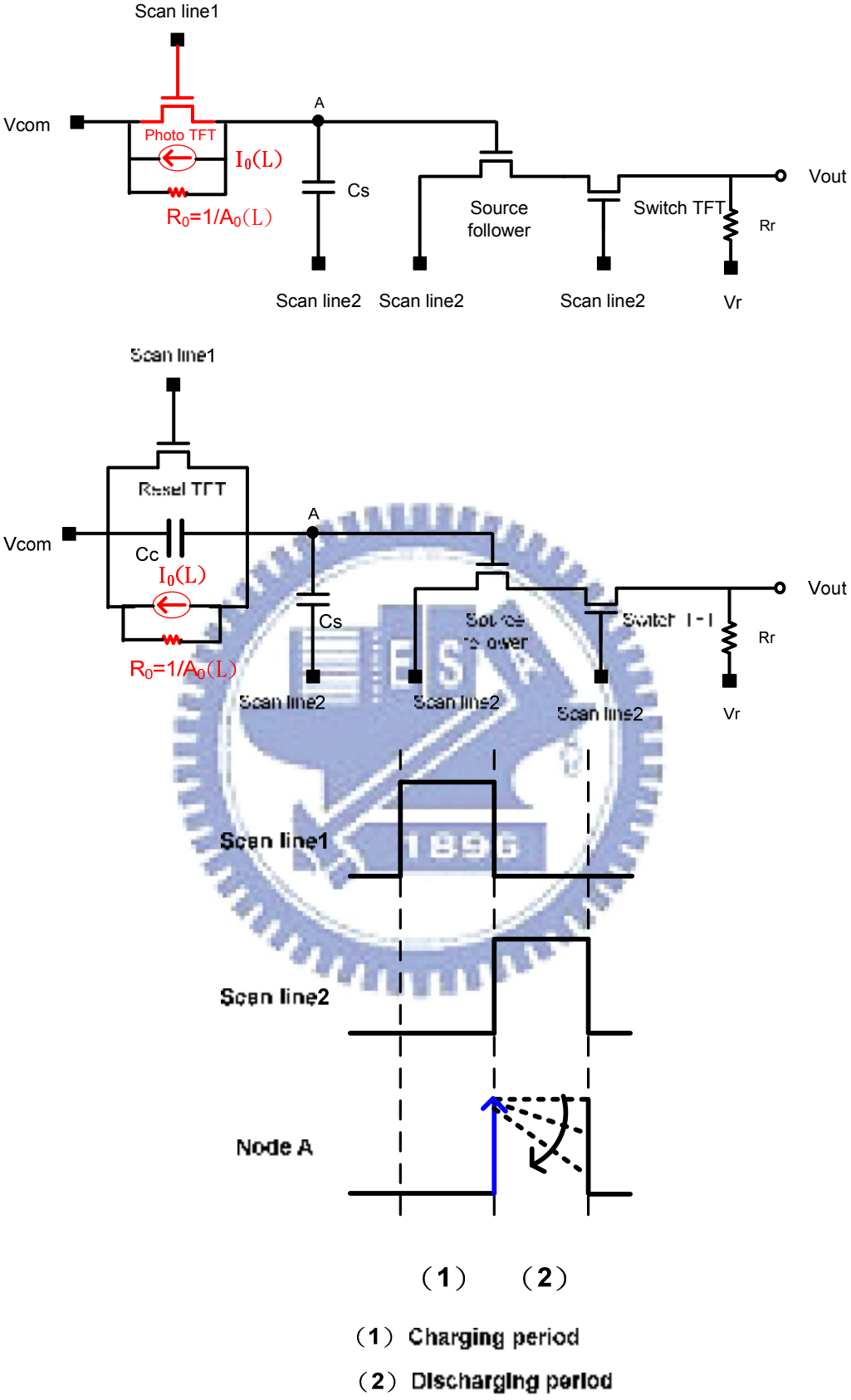

Fig. 3-10 (a) The modified 3T1C light-sensing circuit model for simulation (b) The modified 4T2C light-sensing circuit model for simulation (c) its time diagram.

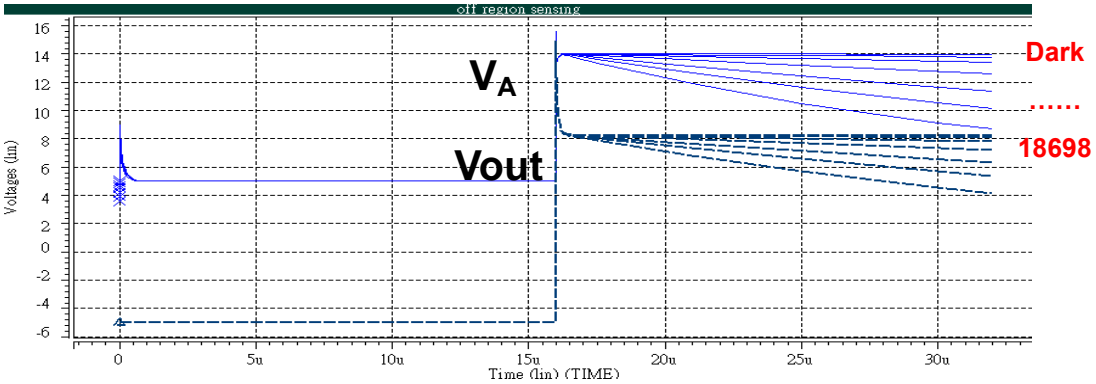

(a)

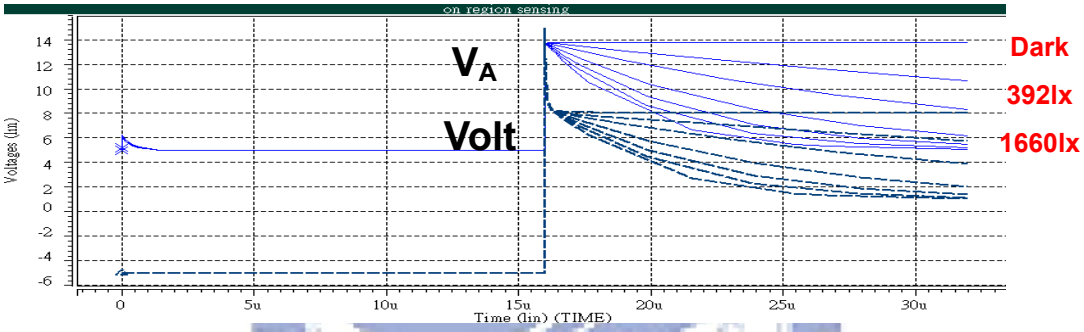

(b)

Fig. 3-11 (a) 3T1C light-sensing circuit model and (b) 4T2C light-sensing circuit model simulation results under illumination and in the dark

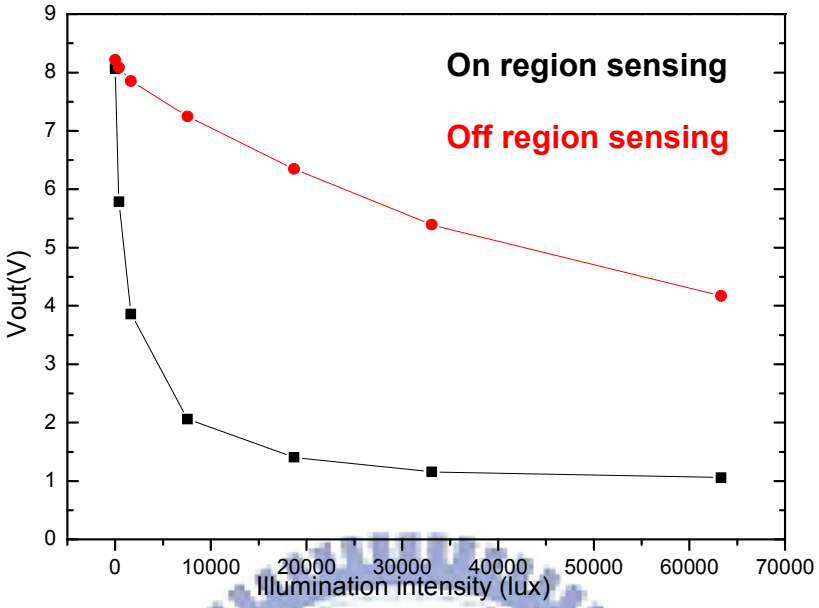

(a)

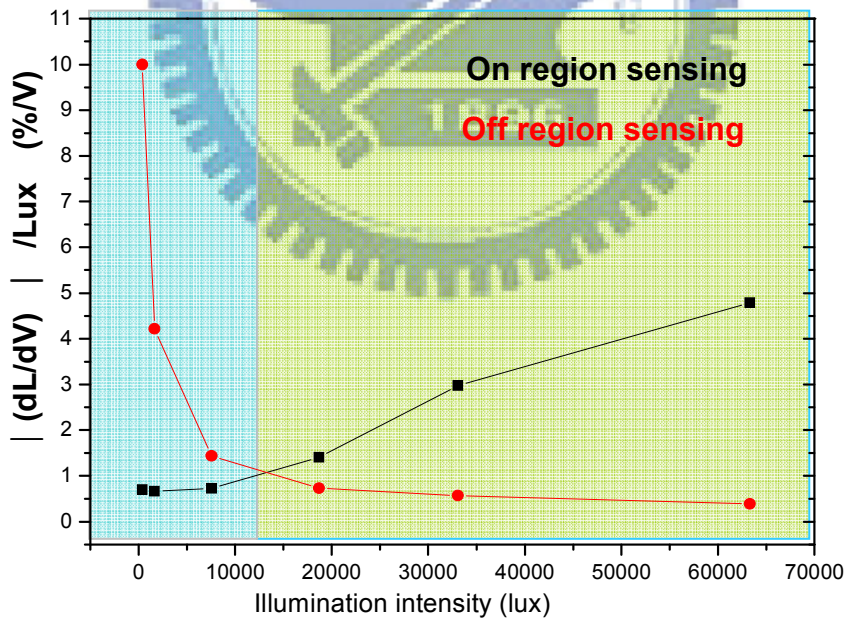

(b)

Fig. 3-12 (a) output voltage and (b) relative error results of the light-sensing circuits under different illumination intensity in ON region and OFF region

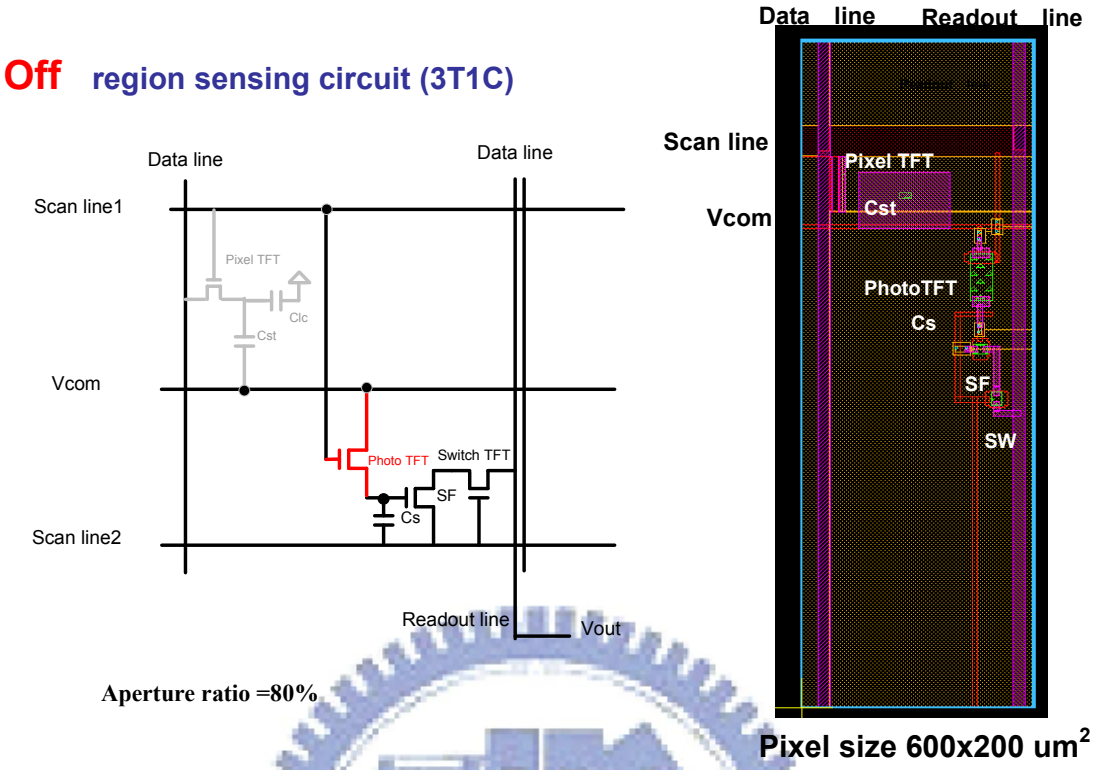

Fig. 3-13 (a) Pixel of the fabricated 3T1C light-sensing circuit

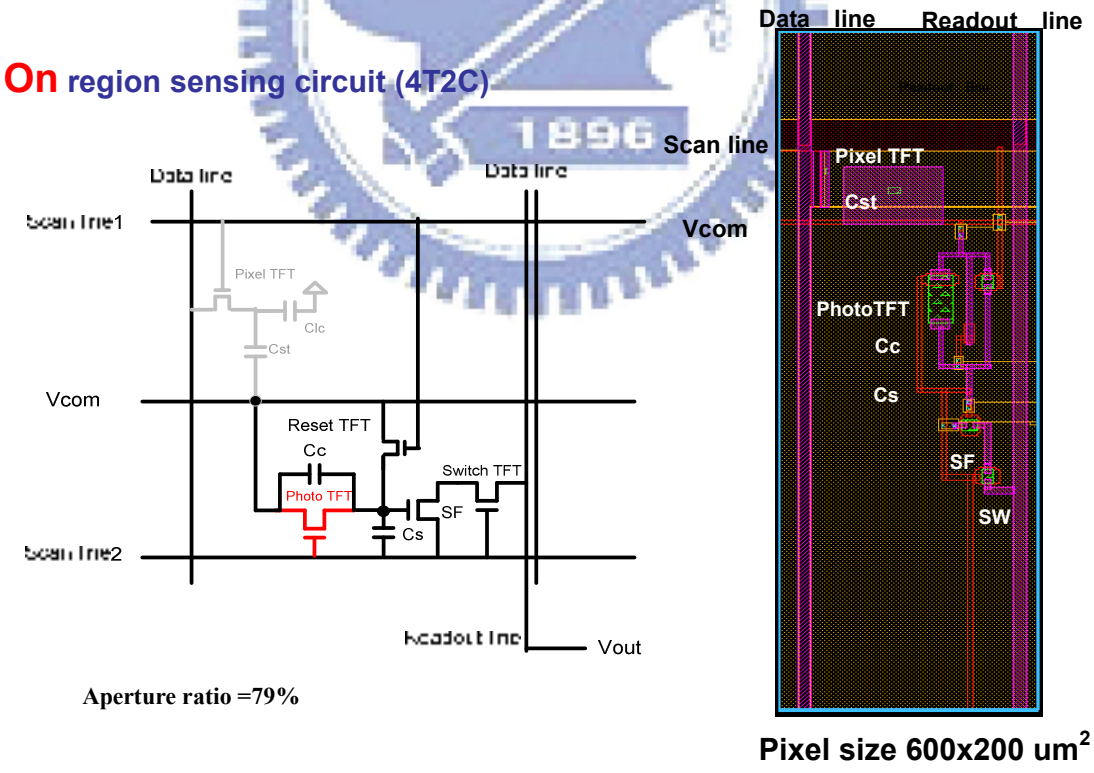

Fig. 3-13 (b) Pixel of the fabricated 4T2C light-sensing circuit

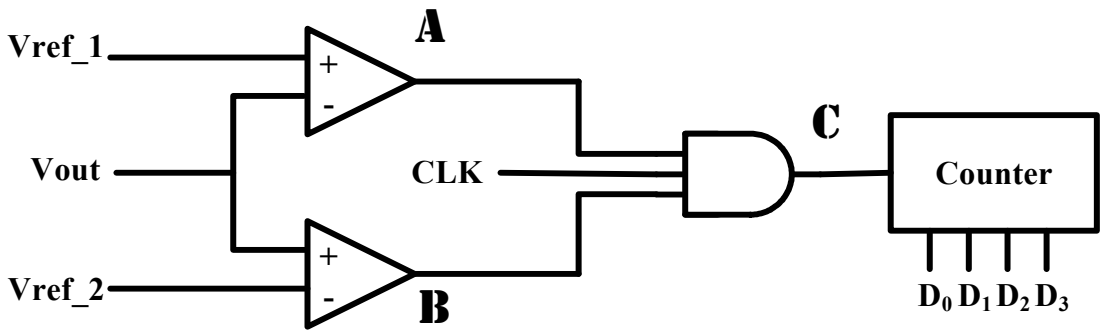

(a)

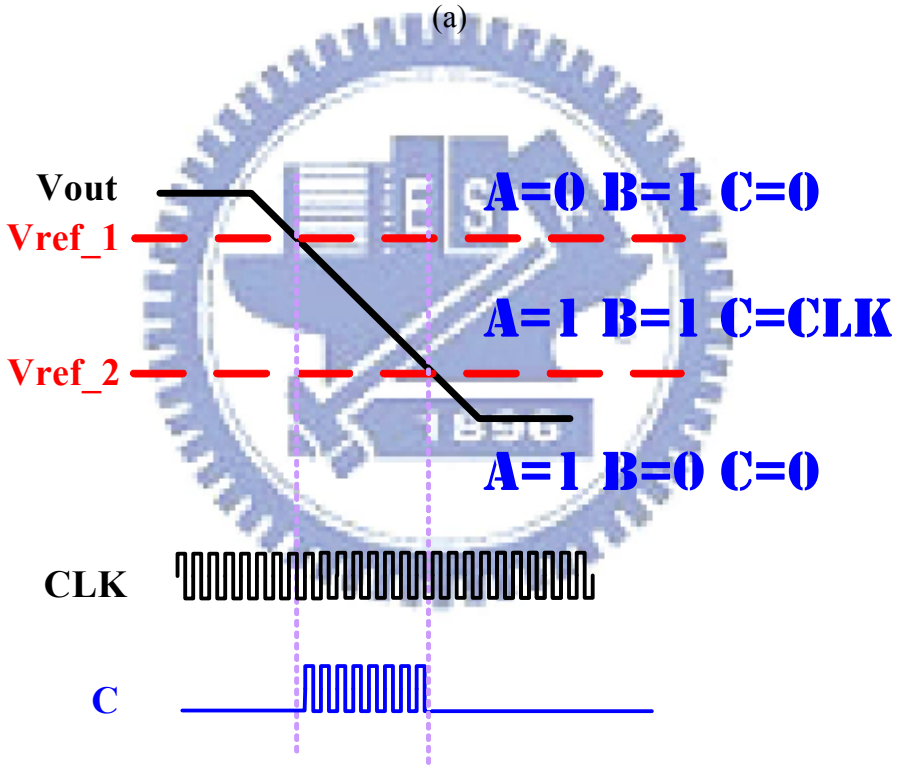

(b)

Fig. 3-14 (a) Simplified block diagram of digitization circuit and (b) its signal diagrams

Chapter 4

Error Factors

4.1 Uniformity

It is clear that for any circuit to be manufacturable, device-to-device uniformity must be controlled. Next, we will discuss this issue for the two types of device variations, namely, OFF current and ON current variation.

Figure 4-1 (a) and (b) show the transfer characteristic curves of photo current versus of illumination intensity at V_{DS}=10V of four a-Si TFTs of Gap-Gate structure for OFF and ON current operation, respectively. We can see the curves have some variation. And we take further steps to analyze the sensing error. Firstly, we average the four measured currents, and take it as the reference standard. Next, we look up the original eight measured data according to the standard one to get the corresponding ambient light intensity, called measured light intensity ($Lux_{measured}$). Moreover, the error which is defined as "$\frac{Lux_{measured}-Lux_{real}}{Lux_{real}}$", is shown in figure 4-2(a) to illustrate the error from OFF current variation. For high level intensity sensing at 63315 lux illumination, it has a maximum error of 1.51%. Figure 4-2(b) shows the error for ON current variation. At 7547 lux illumination in the range of low illumination, it has a maximum error of 4.6%.

4.2 Temperature

In application, the sensor is possibly embedded in TFT array. And the panel's internal temperature is subject to change during using. Thus, we need to consider the temperature effect on device. Assume 40℃ is the panel's normal operating

temperature, and then it happens to vary within the range of ±5℃. Figure 4-3 (a) and (b) show the measured OFF and ON current of device-1 at 35℃、40℃ and 45℃. The error owing to temperature change can be calculated with the same method as that for uniformity. After calculating the errors for four devices , we plot them in figure 4-4 (a) and (b) and find the maximum error exceeds 10% and up to 15.8% at low illumination level for ON region operation. Because the influence from temperature can not be neglected, we take further steps to understand the temperature effect on device.

Figure 4-5(a) shows the ON current versus temperature at different illumination intensities. With the temperature increasing, the drain current also raises gradually [12]. Then we try to fit these curves linearly, and define the slopes as temperature coefficient (TC). Under different illumination intensities, we will get the different TCs. It means that the device does not have the identical response to temperature under different illumination intensities. Figure 4-5(b) is the relation between TC and illumination intensity for four devices. Moreover, we find there is an obvious variation to temperature response from device to device. This phenomenon will cause more difficult in calibration, since it is impossible to calibrate the sensor one by one in the panel. Therefore, we propose to add external to control of the temperature to limit the temperature variation within ±3.5℃. In this case, the maximum error can be controlled to 10% as shown in Figure. 4-5(c) .

4.3 Back Light

If we plan to integrate the photo-sensor into the LCD pixel array, we should consider the photo effect of back light (BL) illumination to simulate its real situation on panel [13-14]. The illumination sources in our measurement include halogen lamp from front side and LED white light from back side as illustrated in figure 4-6.

To discuss on the photo effect of back light illumination, the OFF current and ON current versus the front light (FL) intensity are plotted in figure 4-7(a) and figure 4-7(b), respectively. Also, With a shift in the axis the FL, the corresponding curves for the case with BL are plotted again in the insets together with orginal curves for the case with BL. As can be seen, the pairs of the curves overlap perfectly. It depicts that when we illuminate the device with FL and BL at the same time, the BL intensity of 5070 lux can be equivalent as FL intensity 3690 lux in OFF region and 3624 lux in ON region. Since the BL intensity is fixed in application, we can calibrate the BL effect by the characteristic as mentioned above. Firstly, we take the curve (FL) of the current versus front light as the reference as shown in figure 4-7(a) and figure 4-7(b). Next, we use the originally measured current to look up the illumination intensity according to the reference. This corresponding front light intensity is called $Lux_{measured}$. It is different from the real light intensity (Lux_{real}), as shown by the solid circles in figure 4-8(a) and figure 4-8(b). Another measured intensity can be obtained by subtracting a constant quantity of illumination, which is called calibrated intensity $Lux_{calibration}$. The curves of $Lux_{calibration}$ versus Lux_{real} are also plotted by solid triangles in figure 4-8(a) and figure 4-8(b). We define the error to be "$\frac{Lux_{measured} - Lux_{real}}{Lux_{real}}$". Figure 4-9(a) shows the error from OFF current at high illumination with and without calibration. The error is greatly reduce to have a maximum error 5.26% at 16673 lux illumination. Figure 4-9(b) shows the case of ON current sensing. For low illumination, after calibration it has a maximum error 4.46% at 6683 lux illumination.

The equivalent quantity of intensity shift for the case of OFF region is almost the same as that for the ON region case. If backlight intensity is a constant, we can offset the BL effect during the sensing operation by substrate a constant light intensity, this issue might not so important. In such a case, the photo effect of BL illumination on

the current measurement can be subsided. However, BL induced instability will hinder the sensor operation with BL illumination. This issue will be discussed in section 4.4.3

4.4 Staebler-Wronski Effect

From the study of thin-film hydrogenated amorphous silicon, it is well known that the photo current response of a-Si:H deteriorates under illumination. This property is known as the Staebler-Wronski (SW) effect. The predominant explanation of the effect is that the illumination leads to the creation of additional meta-stable states in the band gap of the amorphous silicon, by breaking the weak bounds of the hydrogen atoms to the silicon, which decreases the lifetime of excess carriers and thus reduces the photoconductivity [15-17].

For presenting the SW effect, we use 20000 lux front light to illuminate the device, and the stress time is from 0 sec to 4800 sec. Figure 4-10 shows that the drain current is almost independent of optical stress time when the Gap-Gate TFT operates in the OFF region. On the other hand, in ON region, we can see the photo current is significantly degradation than that in the OFF-state. For this reason, only the behaviors of ON region in the later sections are considered.

4.4.1 Same Degradation Ratio of FL and BL current under FL Stress

Figure 4-11(a) shows the result after optical stress of 16673 lux front light (FL) from 0 sec to 4800 sec. We can see that with stress time increasing the current degrades obviously. Figure 4-11(b) shows the relationship between the drain current and stress time. It is obvious that the power-law time dependence also appears in our

ON current degradation under optical stress. The illumination drain current is given by:

$$I_{FL}(t) = I_{FL}(0) \times t^{\alpha} . \quad (3)$$

To choose two illumination current I_{FA} and I_{FB} under FL illumination conditions of A (FLA) and B (FLB), we can get:

$$\log[I_{FLA}(t)] = \log[I_{FLA}(0)] + \alpha \log t \ , \quad (4)$$

$$\log[I_{FLB}(t)] = \log[I_{FLB}(0)] + \alpha \log t \ . \quad (5)$$

Subtract equation (5) from equation (4) and we have:

$$\log[\frac{I_{FLA}(t)}{I_{FLB}(t)}] = \log[\frac{I_{FLA}(0)}{I_{FLB}(0)}] \ , \quad (6)$$

or in another form:

$$I_{FLA}(0) = I_{FLB}(0) \times \frac{I_{FLA}(t)}{I_{FLB}(t)} . \quad (7)$$

From equation (7), if $I_{FLB}(0)$ is a reference current measured in a known illumination condition B before optical stress, and we can measure $I_{FLA}(t)$ and $I_{FLB}(t)$ after stress time t. Then, we can trace back the unstress current in condition A current to $I_{FLA}(0)$. Back to our design consideration, we may imagine that there could be two approaches. One is, if FLB is 0 lux, then $I_{FLB}(0)$ can be referenced by controlling the constant backlight illuminating. But in this case, we can not control the sensor to sense only from front light or from the back light alone to retrieve $I_{FLA}(t)$ and $I_{FLB}(t)$ respectively. So, we may resort to another approach. If FLB is a reference front light intensity, then $I_{FLB}(0)$ can also be referenced. But in this case as well we can not control the sensing front light intensity to be equal to the reference intensity to measure $I_{FLB}(t)$. Though the two proposed methods cannot be applied in our sensing circuit, it may be on the other hand applied in the image scanner, only

scan once before operation . But this idea is beyond the scope of this study.

In summary, even though we find an interesting phenomenon of same degradation ratio, it can not be feasibly utilized in real application. We will then propose another calibration method will be described in next section.

4.4.2 Top Metal Shielding Ratio

Figure 4-12(a) shows the device structures with top metal shielding electrode. There is an additional electrode to shield the active region from the front light illumination. No voltage would be applied onto the extra drain. In other words, the electrode is floating. Next, we define the parameter "Open-ratio" for the new structure. For example, the original structure with gap fully illuminated can be described as open_100%. If the area of gap is shielded 67% from the front light illumination, then it would be open_33%. As referred to figure 4-13(a), if we want to implement such kind of devices the structures require the etch stop process to define the extra drain electrode. However, we only have devices using back channel etch (BCE) process as shown figure 4-12(b). Thus, we take an alternative experiment that bottom metal is used to shield the gap from the front light to simulate top metal shielding the front light. Figure 4-13(a) shows the relation between I_{D_illum} and open-ratio at different illumination intensities. It is found that I_{D_illum} is proportional to the open-ratio. It means that the photo effect is proportional to the illuminated area of the gap. But this phenomenon could change after illumination stress. Since the larger open-ratio of the gap area is subject to more optical stress, the different degrees of stress causes the nonlinear behavior as shown in figure 4-13(b). From the nonlinear behavior, we observe an interesting phenomenon and develop a calibration method to be describle below:

4.4.3 Without Back light Stress

Before introducing the calibration method, we define the I_D/Open-ratio as the new index. The I_D/Open-ratio versus open-ratio before stress is shown in figure 4-14(a). We can see the I_D/Open-ratio is independent of open-ratio before stress. Since the device degraded level associates with illuminated intensity, stress time as well as illuminated area, it implies that the larger open-ratio structure will degrade more serious. Figure 4-14(b) shows curves of the stressed devices. The one with open ratio of 100% degrades most seriously. The smaller open-ratio structure subjects to smaller influence from SW effect. The first idea coming to mind is finding open-0% structure which means it will not be stressed by front light.

Since there is no open-0% structure of gap-type TFT, which will become conventional TFT and insensitive to backlight, we need to extrapolate it by the other structures with different open ratios. Now we explain the procedure of calibration for the sensing of the 50000 lux front light as an example. Figure 4-15(a) shows the curve of I_D/Open-ratio versus open ratio for various stress times. We use a formula in the form **Y=A+B*exp^(-x/C)** by OriginPro software to extrapolate the case of 0% stress. To obtain the case of 0% stress, the x, which represents open ratio, is replaced by 0. Thus, the exponential item in formula always be 1. Therefore, the I_D/Open-ratio without optical stress, which is represented by y, would be the sum of coefficient a and coefficient b. For various stress time, all the extrapolations give almost the same I_D/Open-ratio value of 7.73×10^{-8} ($\pm$ 1.68×10^{-9}) (A/%). Since this value is independent of stress time, we take advantage of this unique phenomenon for calibration. Looking back to refer to figure 4-14(a), this stress time independent I_D/Open-ratio value corresponds to the illumination intensity of 48836 ($\pm$ 2986) lux, which is very close to

the real illumination intensity. For other cases, we can also use this extrapolation method to obtain the corresponding 0% cases. Then, we transfer the obtained value to corresponding light intensity according to the curve in figure 4-14(a). Next, we do the error analysis between the measured light intensity, also called calibrated light intensity, and the really illuminated intensity. The error defined as $\frac{\text{Lux}_{\text{measured}} - \text{Lux}_{\text{Real}}}{\text{Lux}_{\text{Real}}}$. We can see the maximum error, shows in figure 4-15(b), can be reduced to about 13.6%. This result indicates that the calibration method is very effective to lower the SW influence.

In reality, the ambient light intensity may not be always the same. Therefore, it would be of practical interest to check the calibration method, as mentioned above, under various front light stress condition. The device is stressed by l0000 lux front light from 0 to 3600 seconds, and then stressed by l9160 lux front light from 3600 to 7200 seconds. Because of the different stressed intensities, the curves present two different degradation trend. Figure 4-16(a) shows the drain current versus stress time. We also use the same proposed method to calibrate the SW effect, as shown in figure 4-16(b). Similarly, the error analysis, as shown in figure 4-16(c), reveals that the proposed method can effectively reduce the SW effect on the device.

4.4.4 With Back light Stress

In order to integrate the photo-sensor into the pixel, the Steabler-Wronski effect of back light (BL) illumination should be considered to simulate the operation conditions in real applications. In reality, the Steable-Wronski effect would occur for both the ambient light and back light. Therefore, we want to see the validity of the calibration, as mentioned above, under both the front light and back light stress. The device is thus stressed by 19160 lux front light and 16673 lux back light from 0 to

4800 seconds. Figure 4-17(a) shows the relationship between the drain current and stress time. The same calibration method is also utilized to calibrate the SW effect, as shown in figure 4-17(b). Before stress, I_D/Open-ratio is no longer a constant because of the constant back light stress. So we want to subtract the current under constant back light. But this current is no longer a constant after stress because of Steabler-Wronski effect. So as for our calibration method we can not extrapolate the case of 0%, which corresponds to the case without Steabler-Wronski effect.

4.5 Discussion

After proposing calibration of SW effect, we assessed the application of our front light sensor. The Steabler-Wronski effect can be offset by top metal shielding, but the Steabler-Wronski effect from ambient light and back light. For sensing front light accurately, the sensing TFT must be avoid back light effect, and figure 4-18 is the schematic diagram. We place the ambient light sensor around the monitor without backlight. Meanwhile, it also can avoid the optical stress from back light. If there has back light, the device could be stressed by not only front light but also backlight. And it will cause our proposed calibration failed. Moreover, in our calibration of SW effect, we need to use multiple devices with different open-ratio.

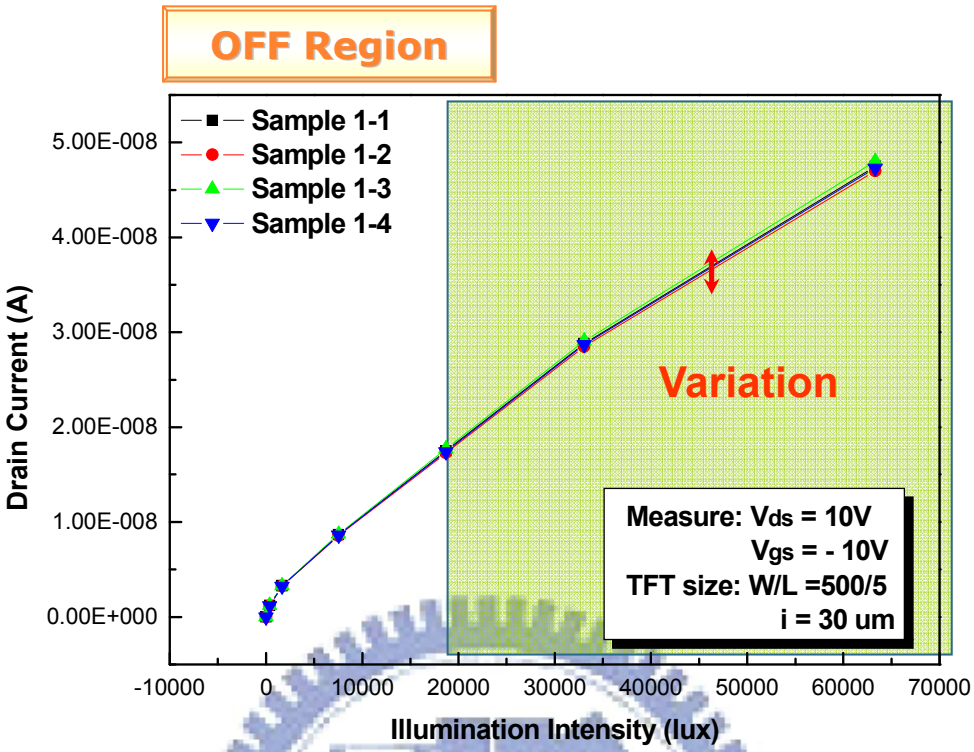

Fig. 4-1(a) OFF current variations of a-Si TFTs of 4 devices.

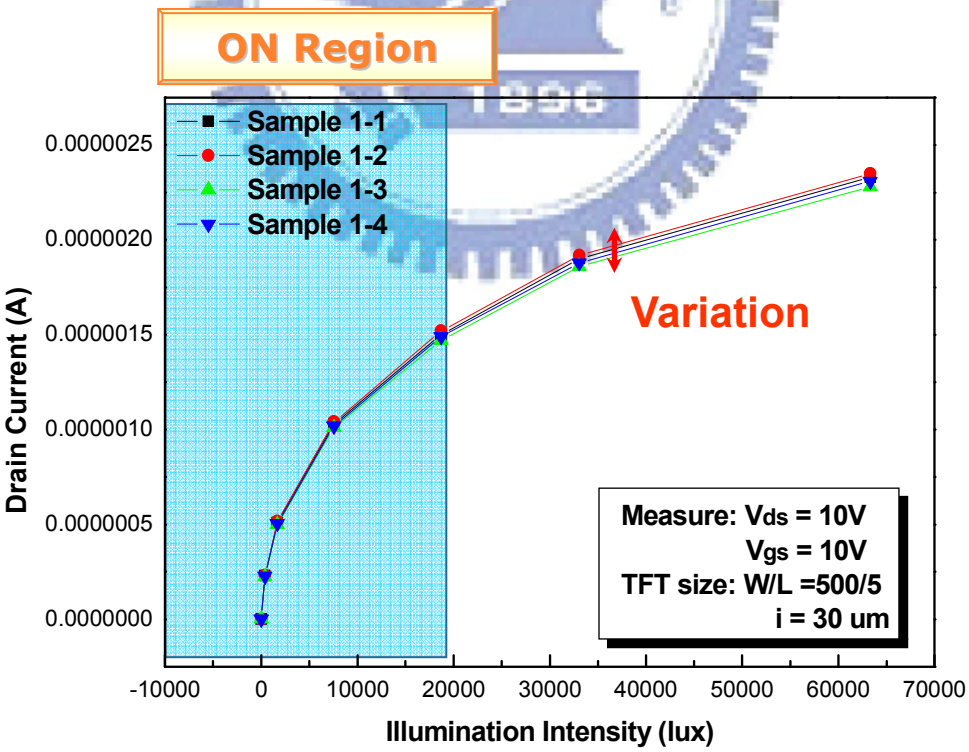

Fig. 4-1(b) ON current variations of a-Si TFTs of 4 devices.

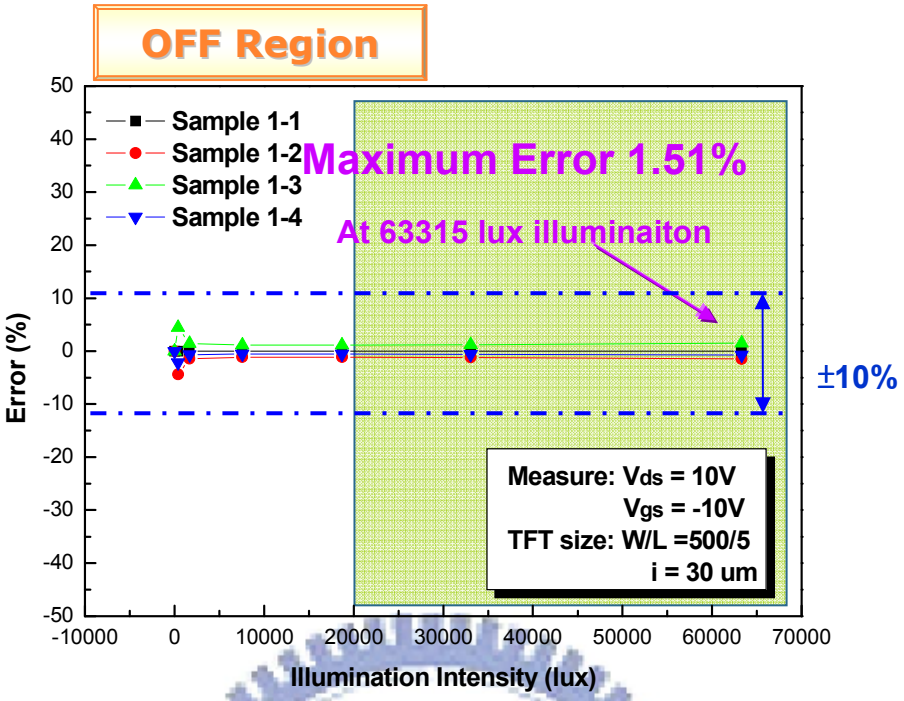

(a)

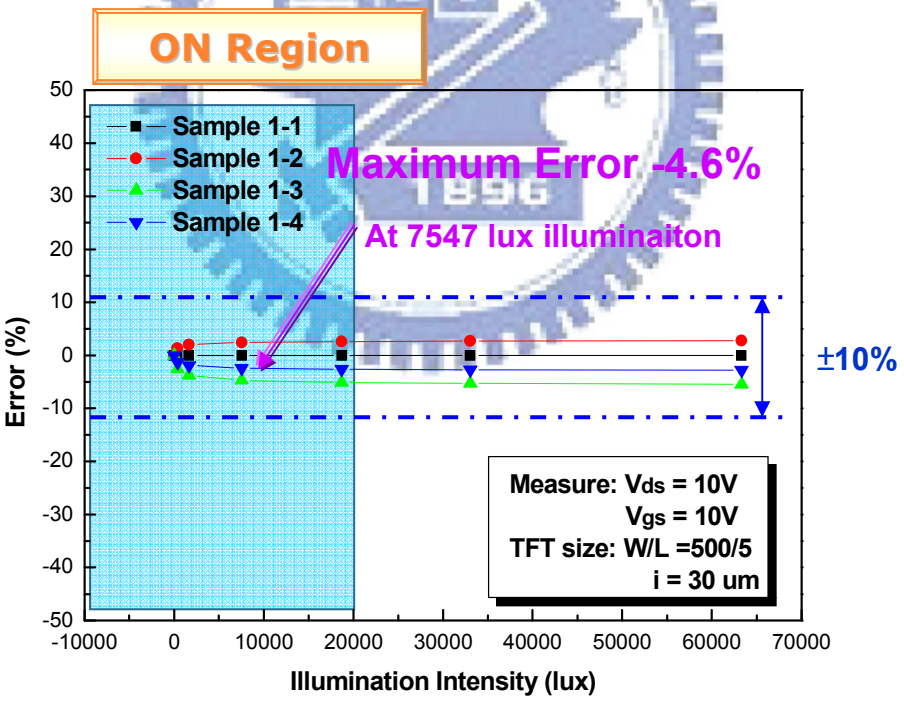

(b)

Fig. 4-2 Error analysis of ON current variation between the measured light intensity and the illuminated light intensity.

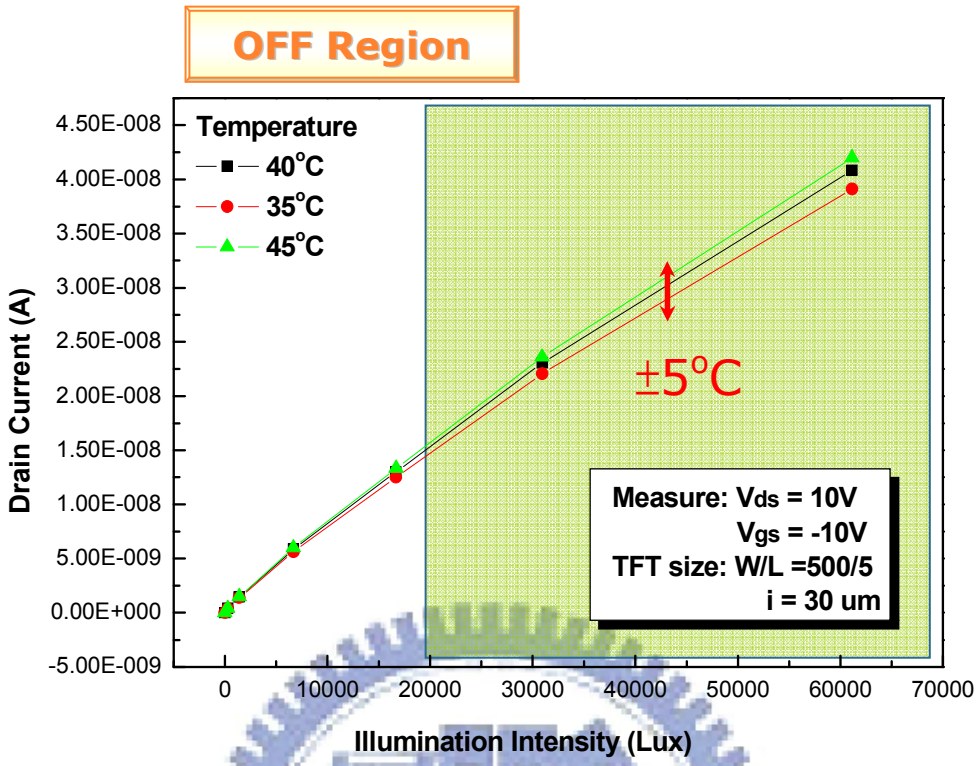

Fig. 4-3(a) The OFF current versus illumination intensity at 35℃, 40℃, and 45 ℃.

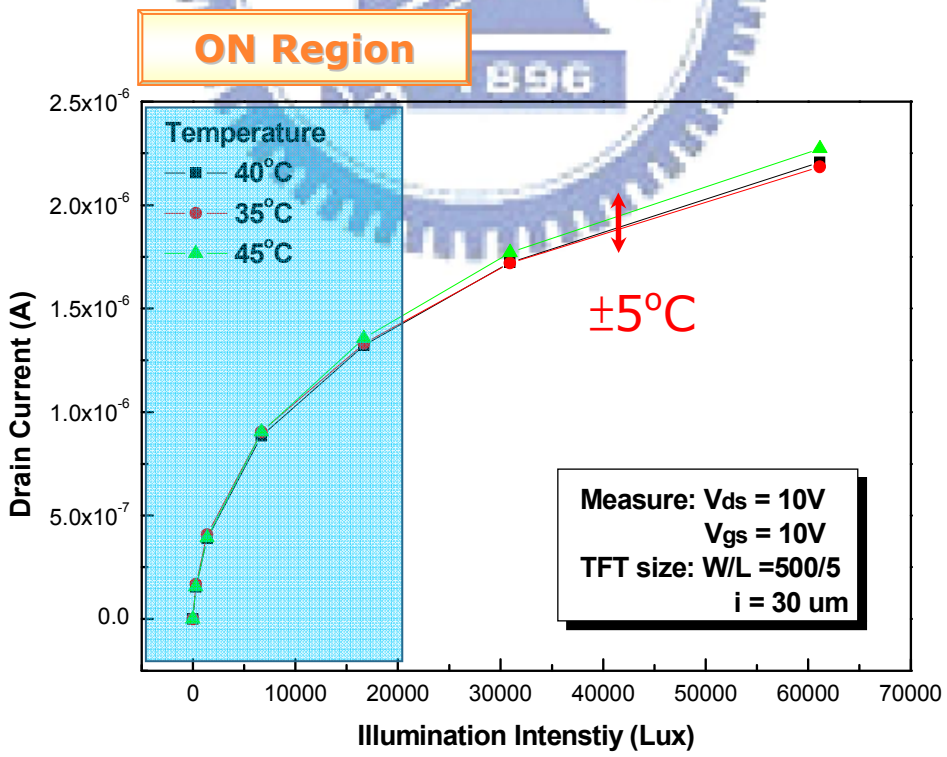

Fig. 4-3(b) The ON current versus illumination intensity at 35℃, 40℃, and 45 ℃.

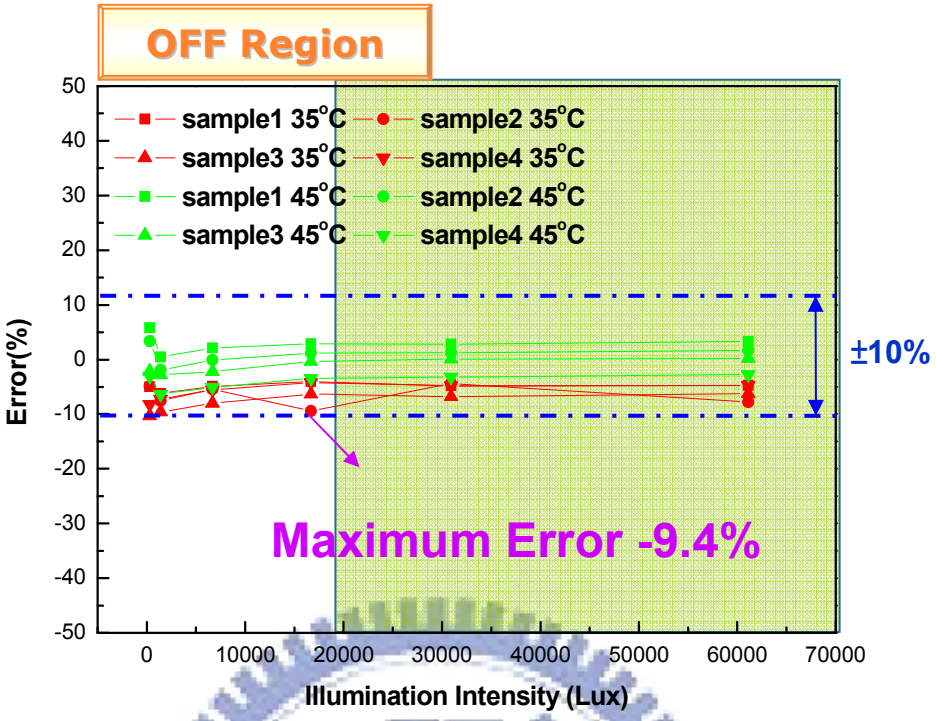

(a)

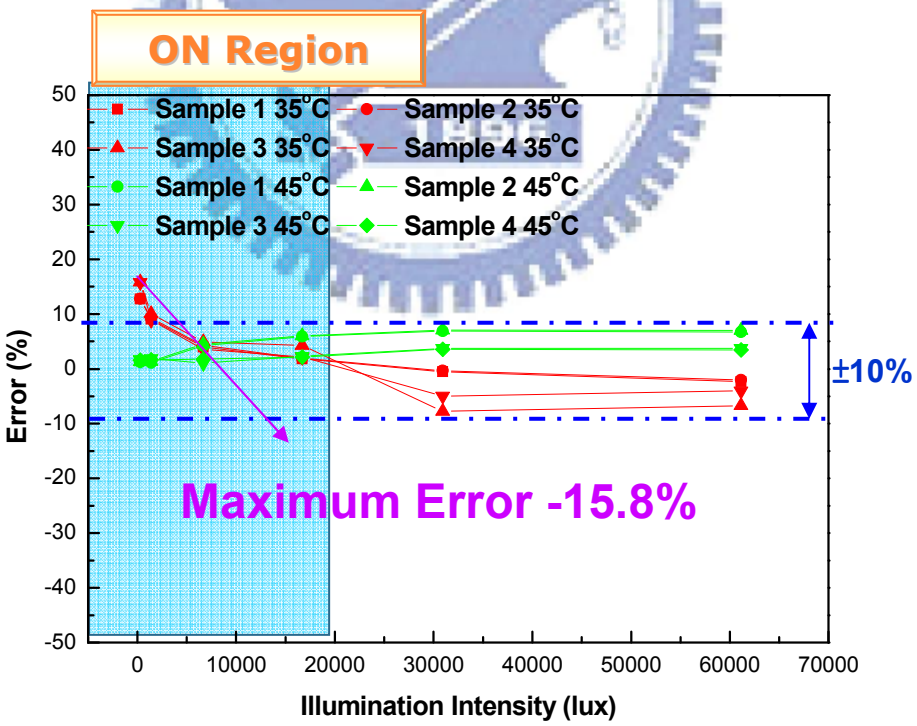

(b)

Fig. 4-4 Error analysis of temperature variation (±5℃) between the measured light intensity and the illuminated light intensity in (a) OFF region and (b) ON region

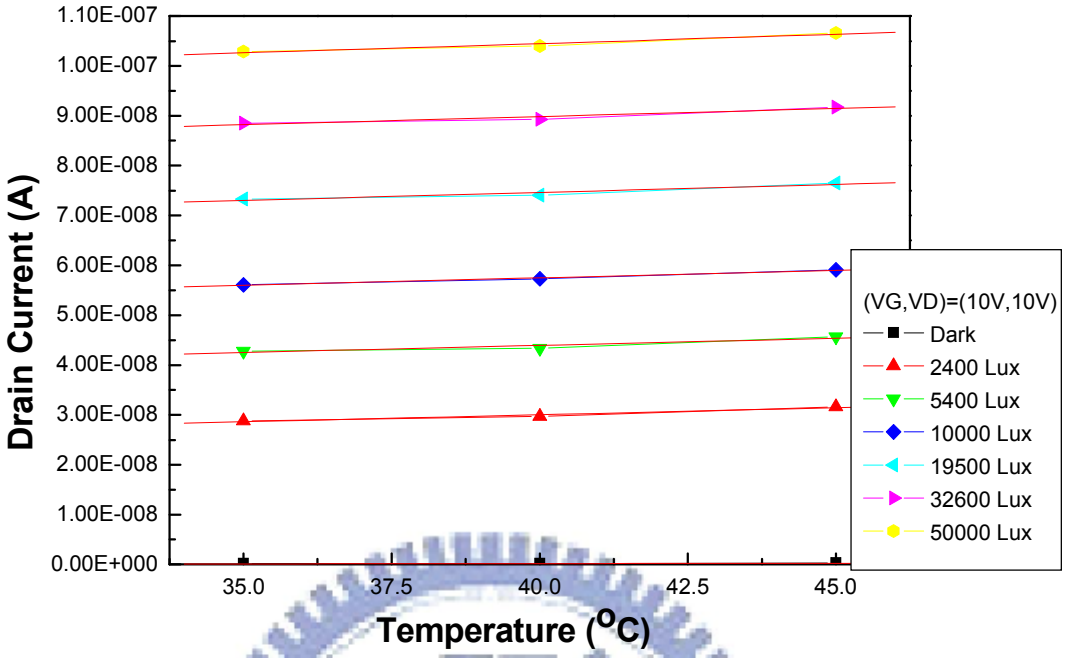

Fig. 4-5 (a) The ON current versus temperature at Vgs=10V, Vds = 10V

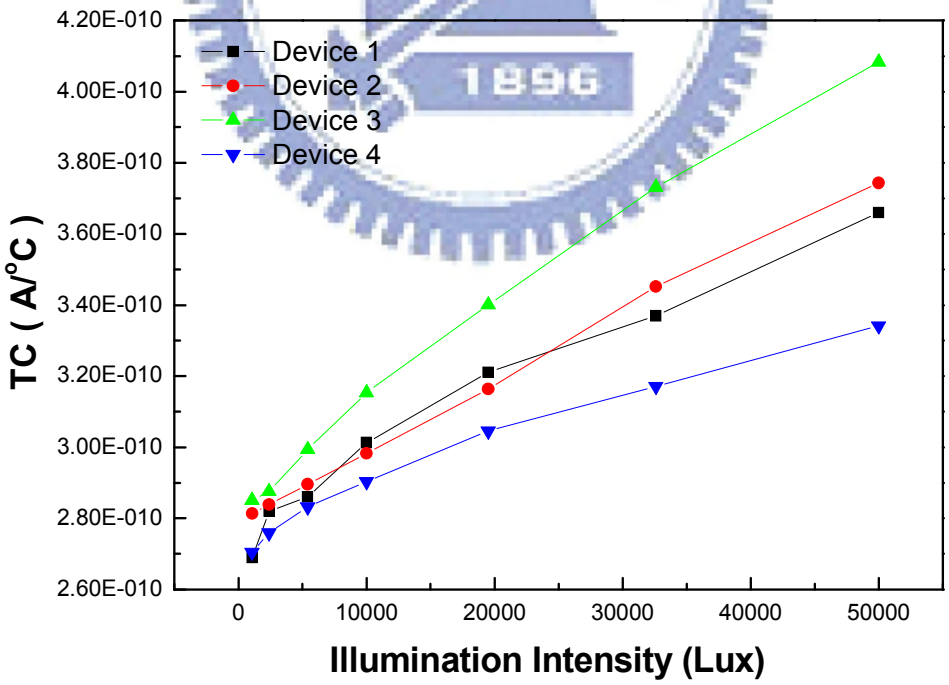

Fig. 4-5 (b) The temperature coefficient versus temperature curves of 4 devices

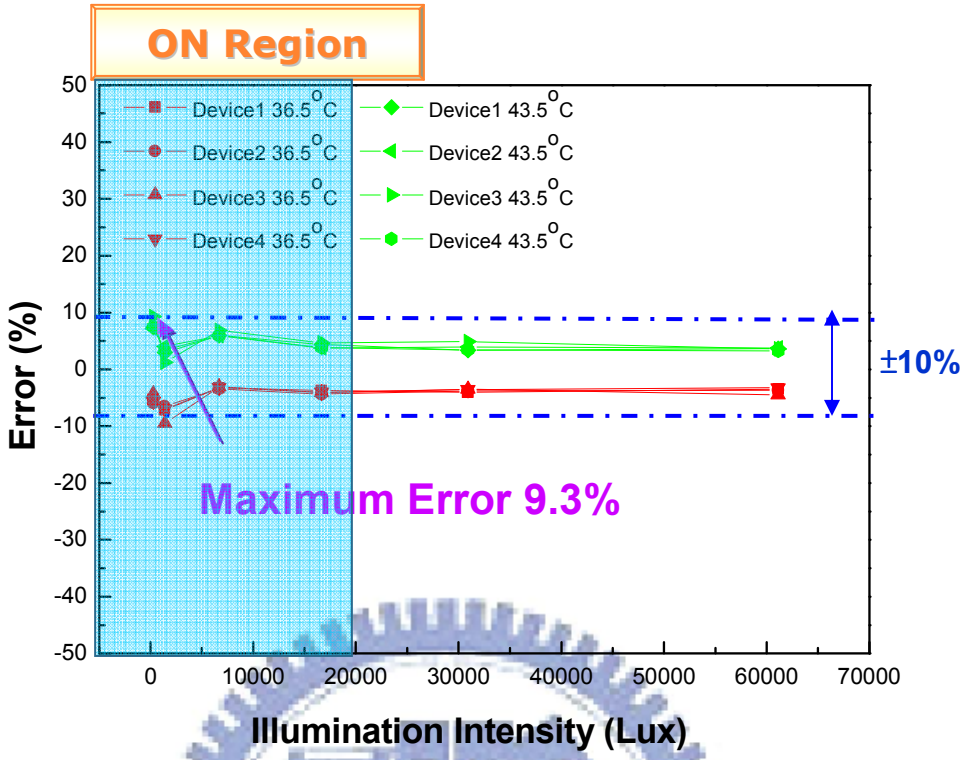

Fig. 4-5 (c) Error analysis of temperature variation (±3.5℃) between the measured light intensity and the illuminated light intensity in ON region

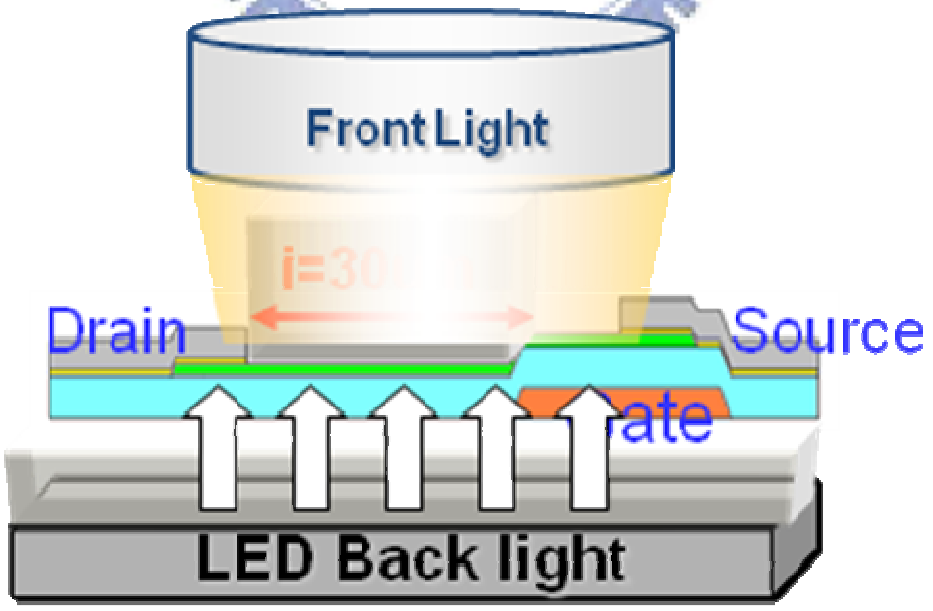

Fig. 4-6 Simulate a-Si TFT's real situation on panel.

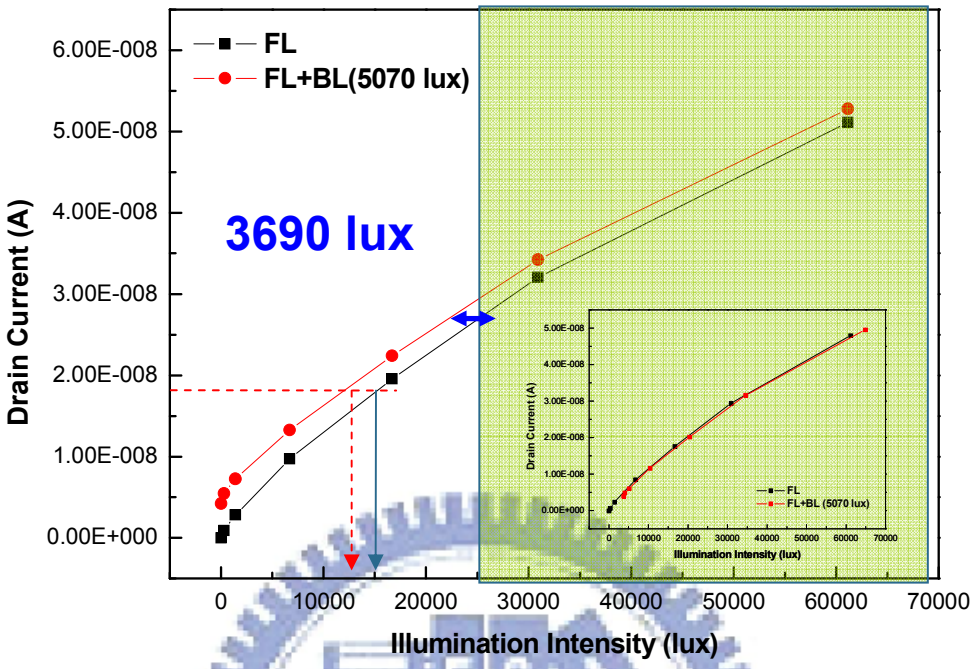

Fig. 4-7 (a) The OFF current versus FL illumination intensity without BL and with BL

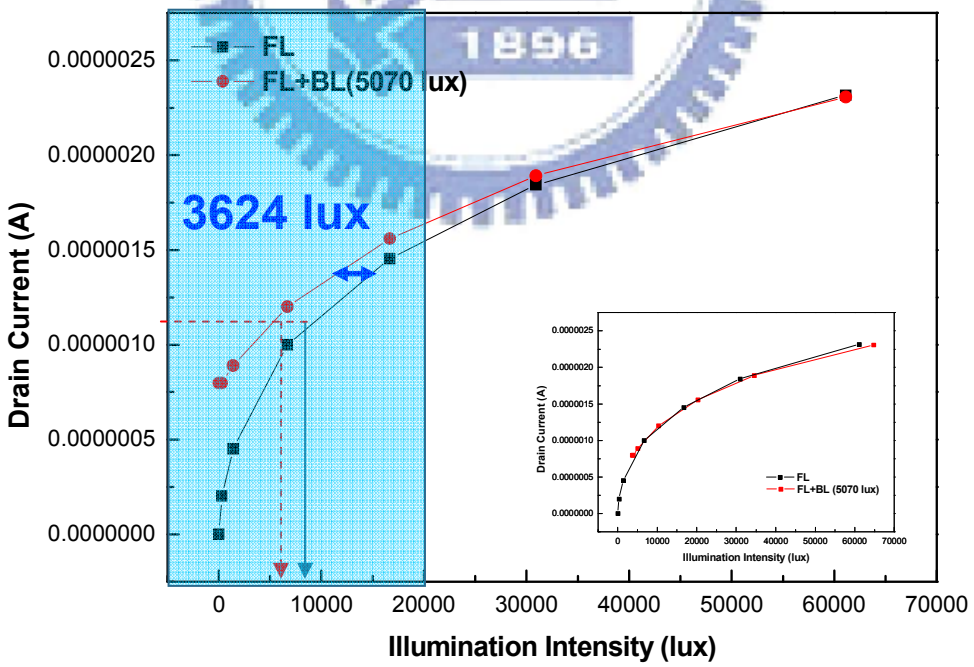

Fig. 4-7 (b) The ON current versus FL illumination intensity without BL and with BL

$$Lux_{calibration} = Lux_{measured} - 3690$$

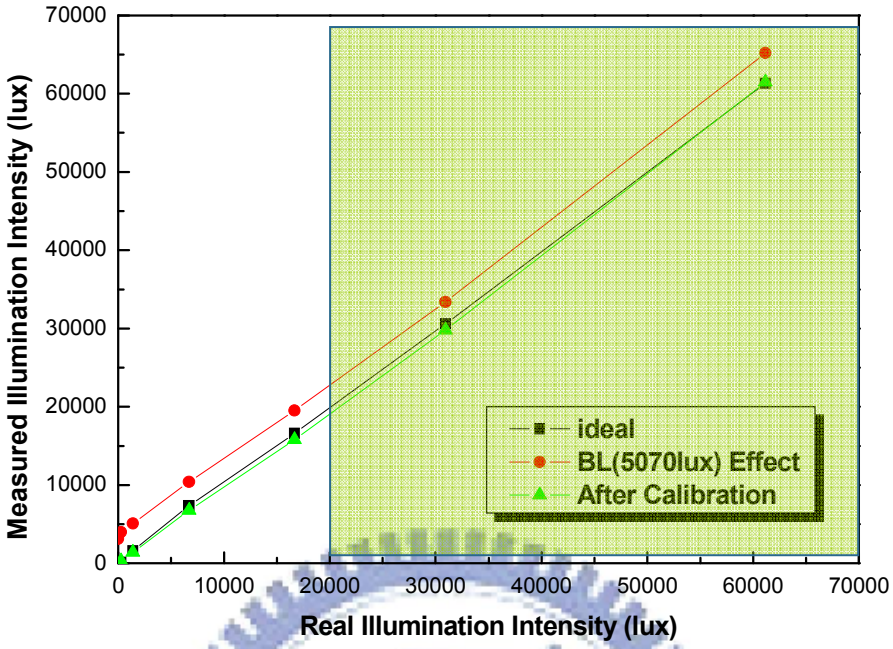

(a)

$$Lux_{calibration} = Lux_{measured} - 3624$$

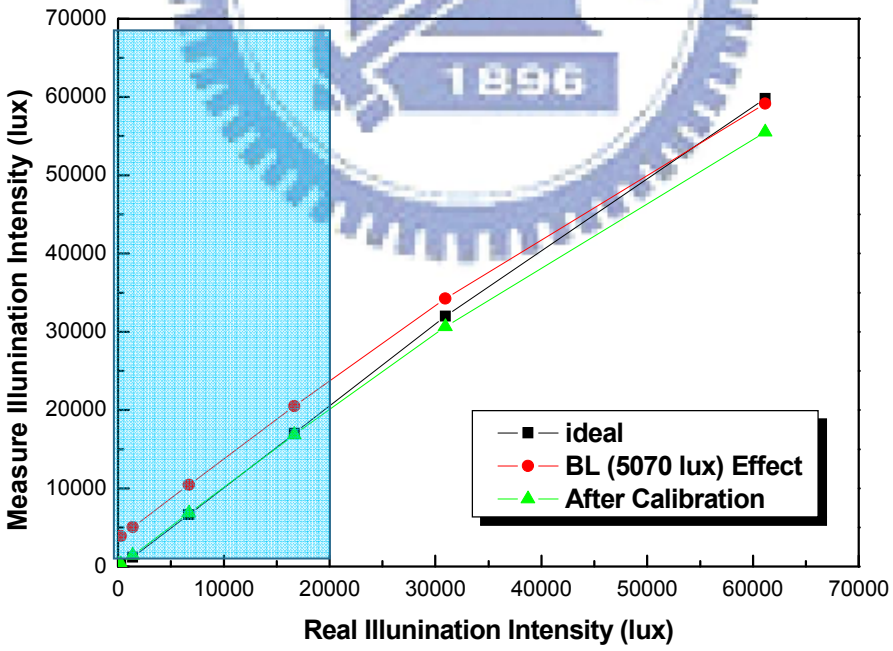

(b)

Fig. 4-8 The relation between the measured light intensity and the illuminated light intensity in (a) OFF region and (b) ON region

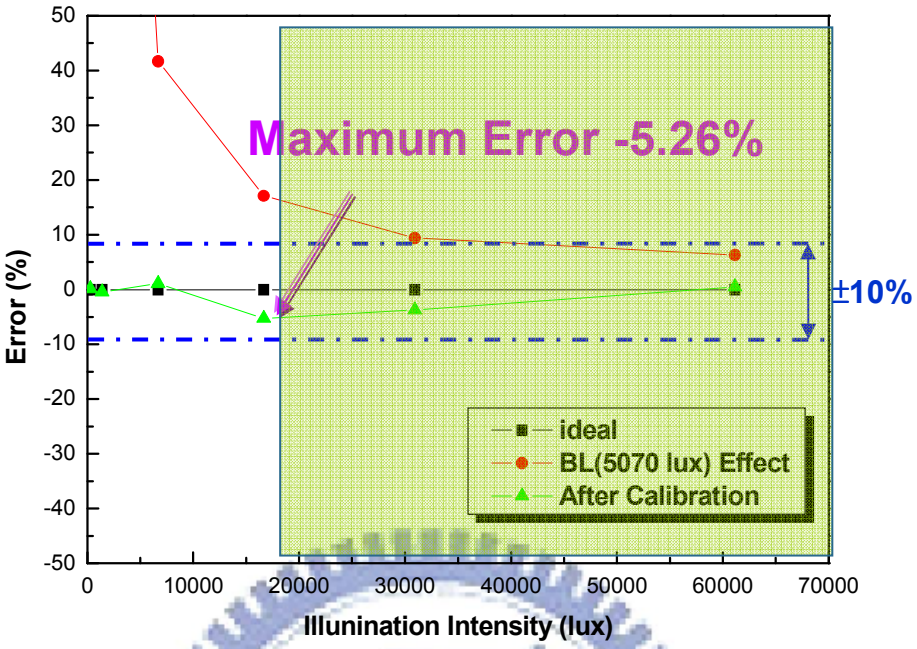

(a)

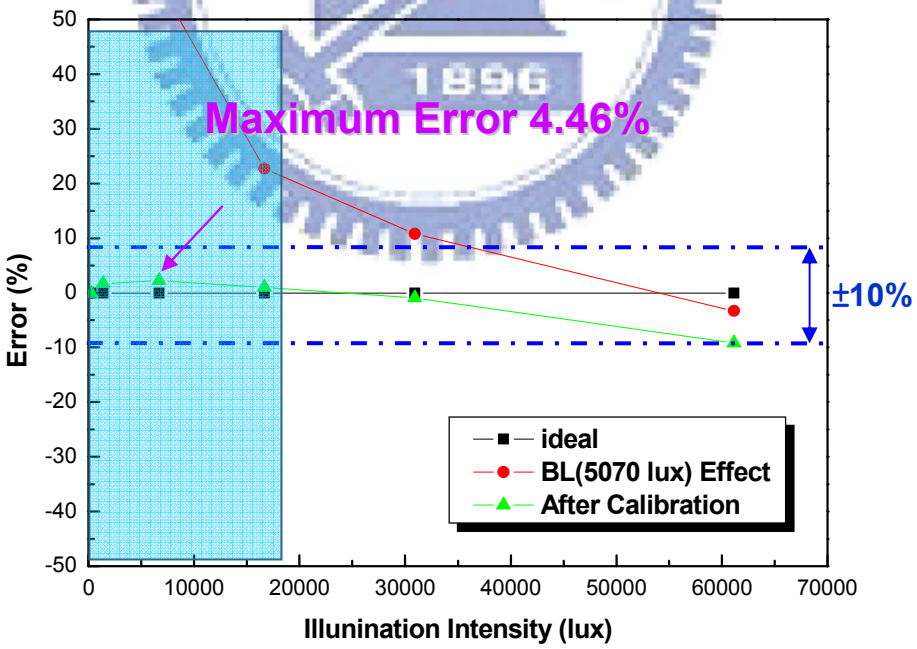

(b)

Fig. 4-9 Error analysis of backlight effect between the measured light intensity and the illuminated light intensity in (a) OFF region and (b) ON region

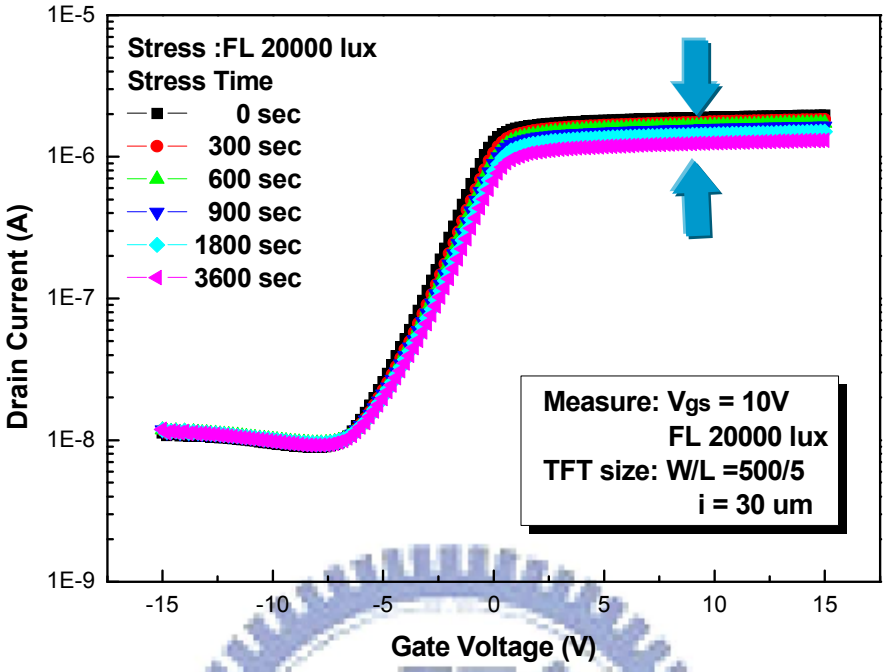

Fig. 4-10 (a) Gap gate TFT transfer characteristics with SW effect at V_{DS}=10V

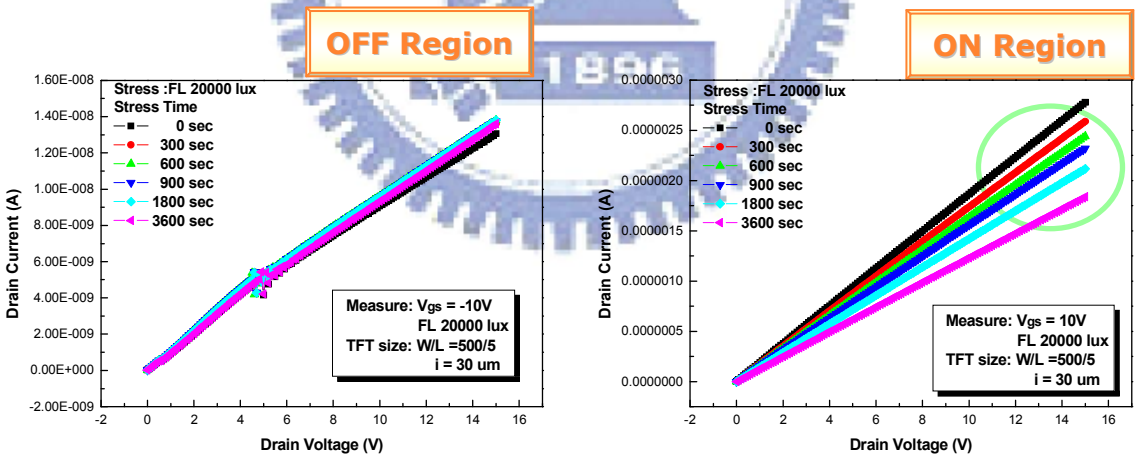

Fig. 4-10 (b) I_D-V_D characteristics of OFF region and ON region with SW effect

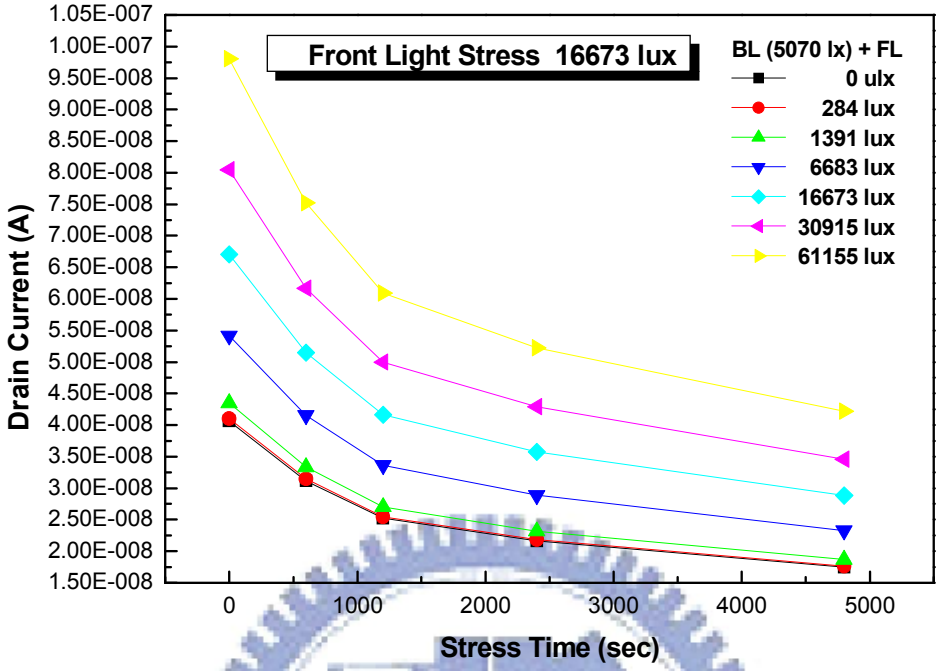

Fig. 4-11 (a) Drain current versus front light stress time with different intensity

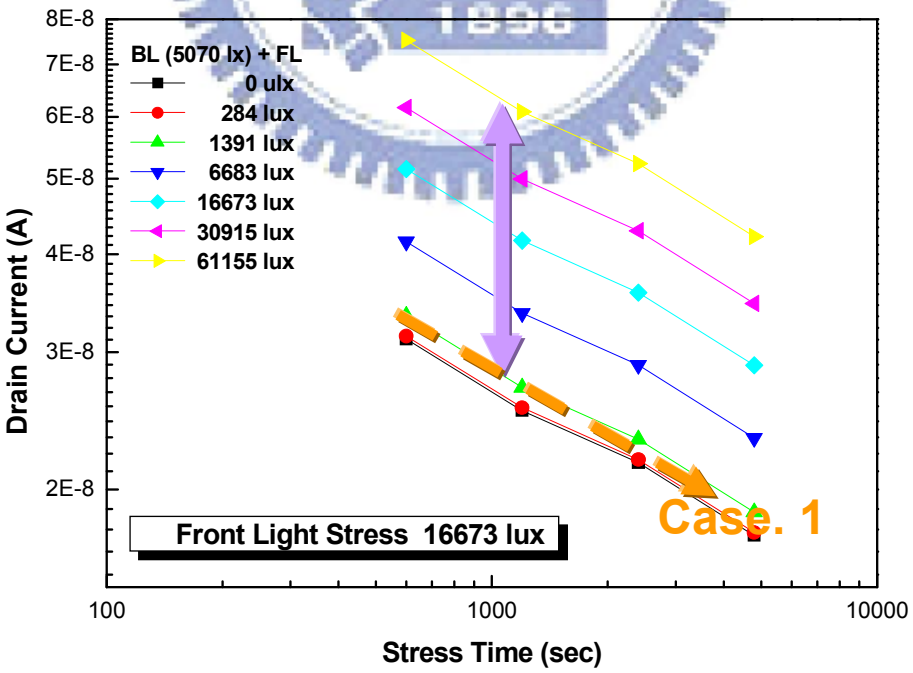

Fig. 4-11 (b) The power-law time dependence between drain current and stress time

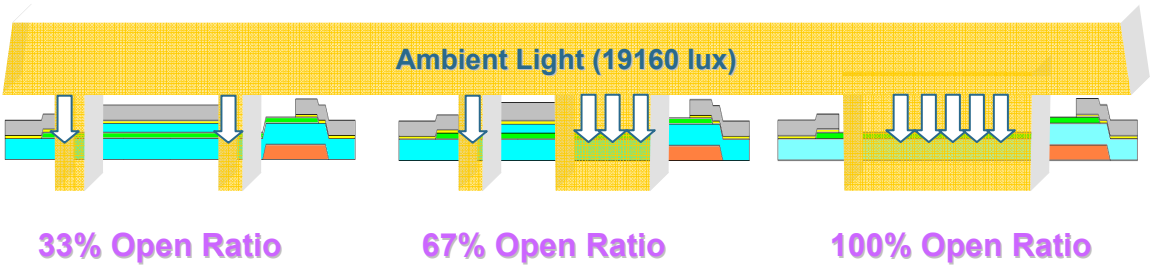

Fig. 4-12 (a) The top metal floating shielding (ES process)

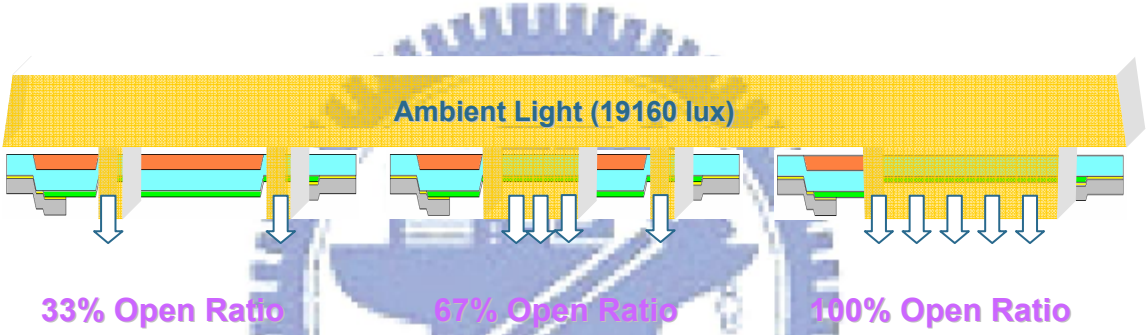

Fig. 4-12 (b) The inverted bottom metal floating shielding (BCE process) simulating the top metal shielding devices

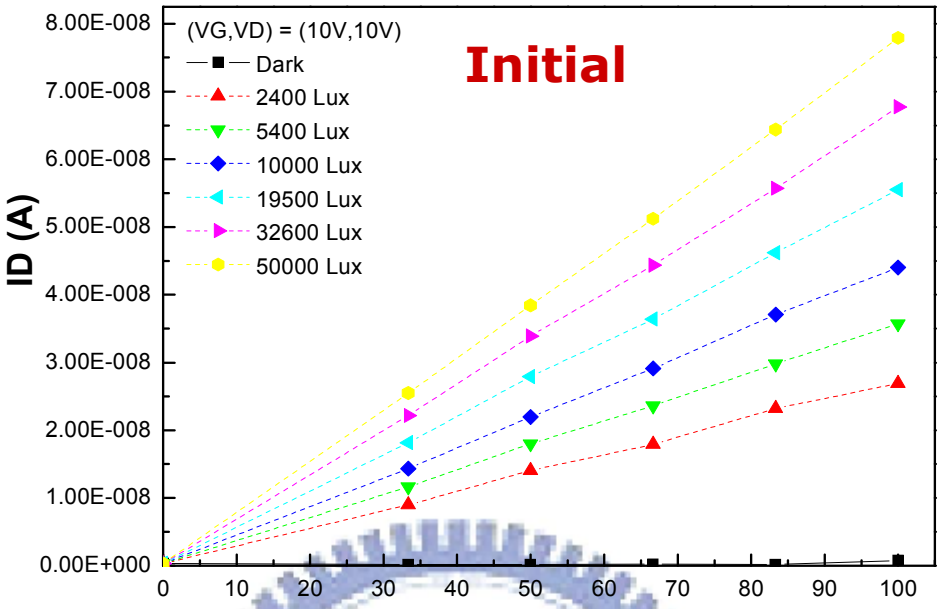

(a)

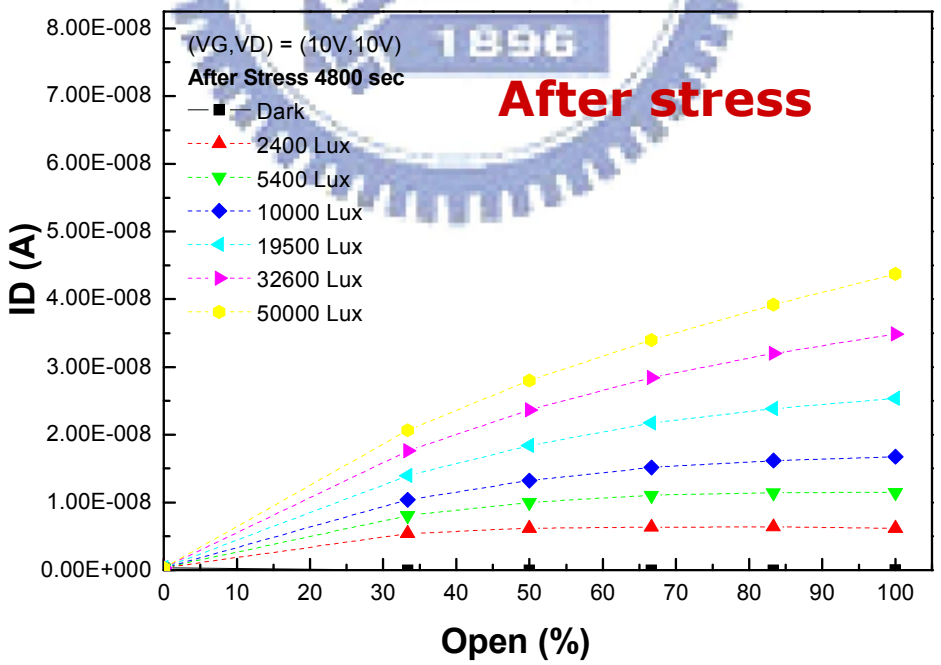

(b)

Fig. 4-13 Drain current versus open ratio (a) before stress and (b) after stress

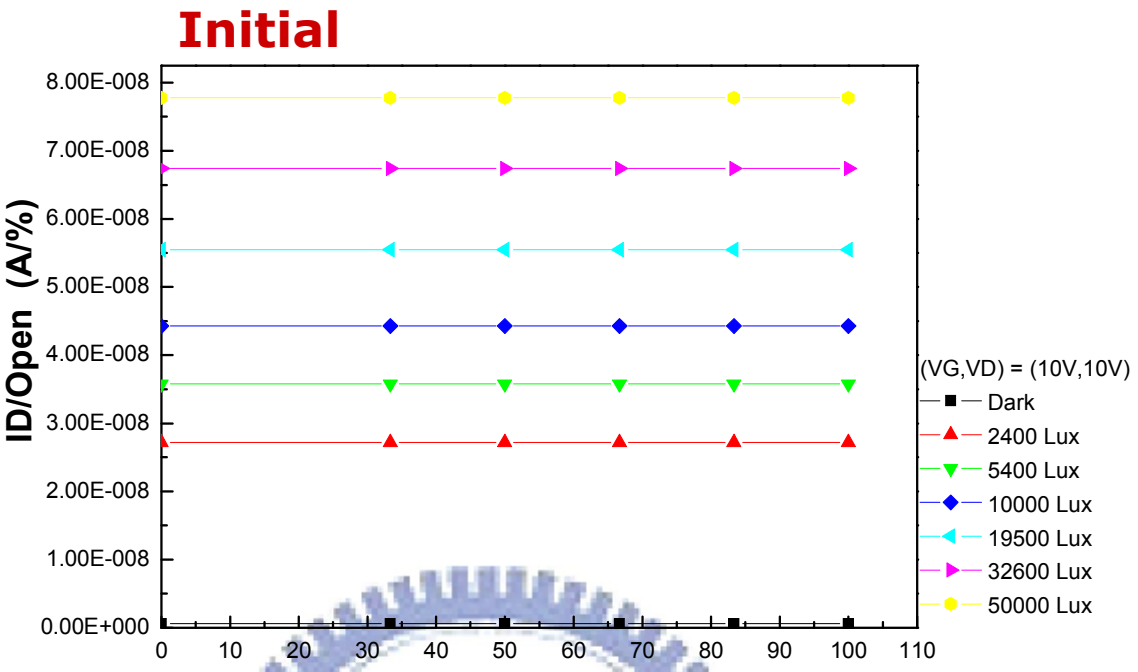

(a)

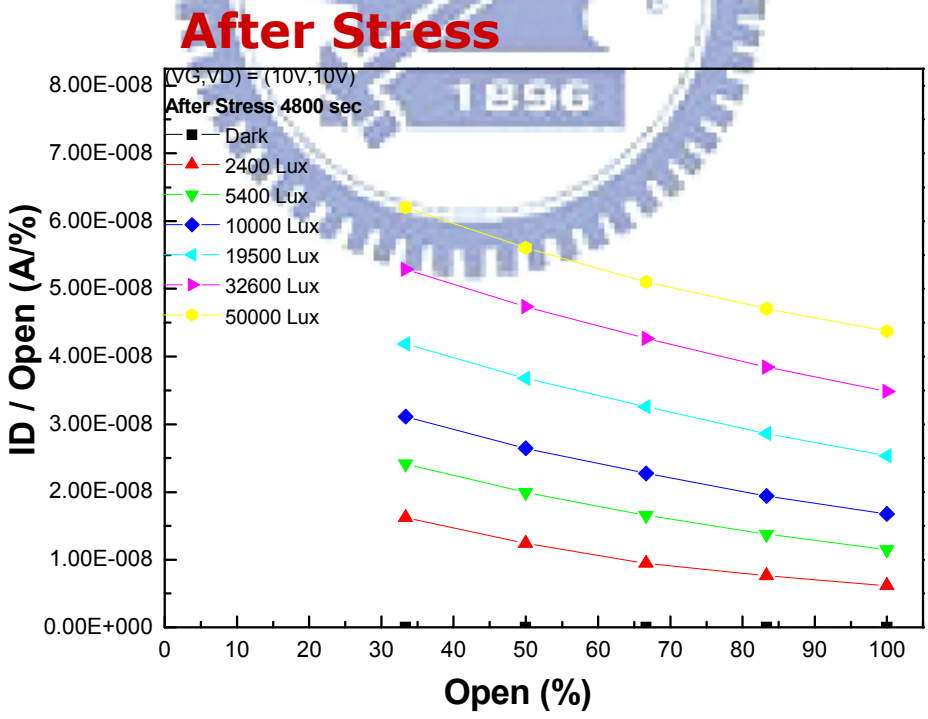

(b)

Fig. 4-14 The I_D/Open-ratio versus open-ratio (a) before stress and (b) after stress

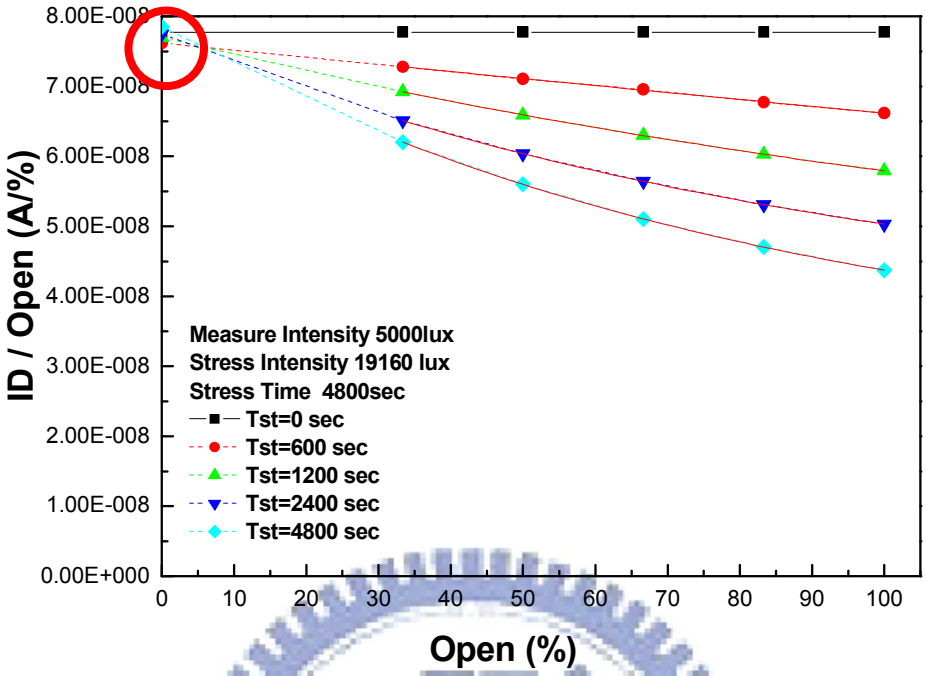

Fig. 4-15 (a) I_D/Open-ratio versus open-ratio under 50000 lux illumination with different stress times

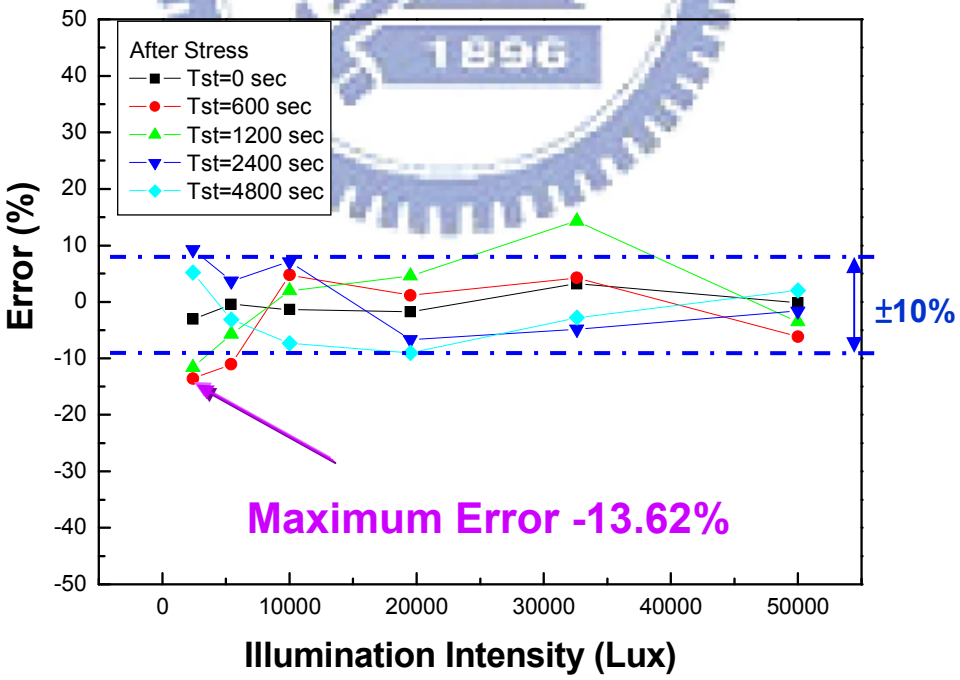

Fig. 4-15 (b) Error analysis of SW effect after calibration between the measured light intensity and the illuminated light intensity

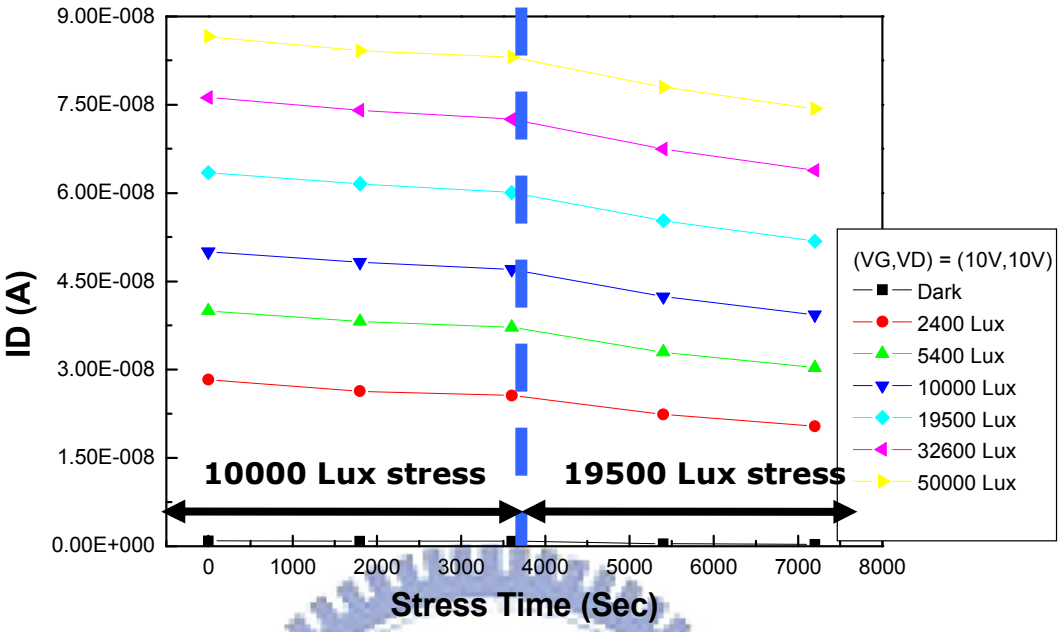

(a)

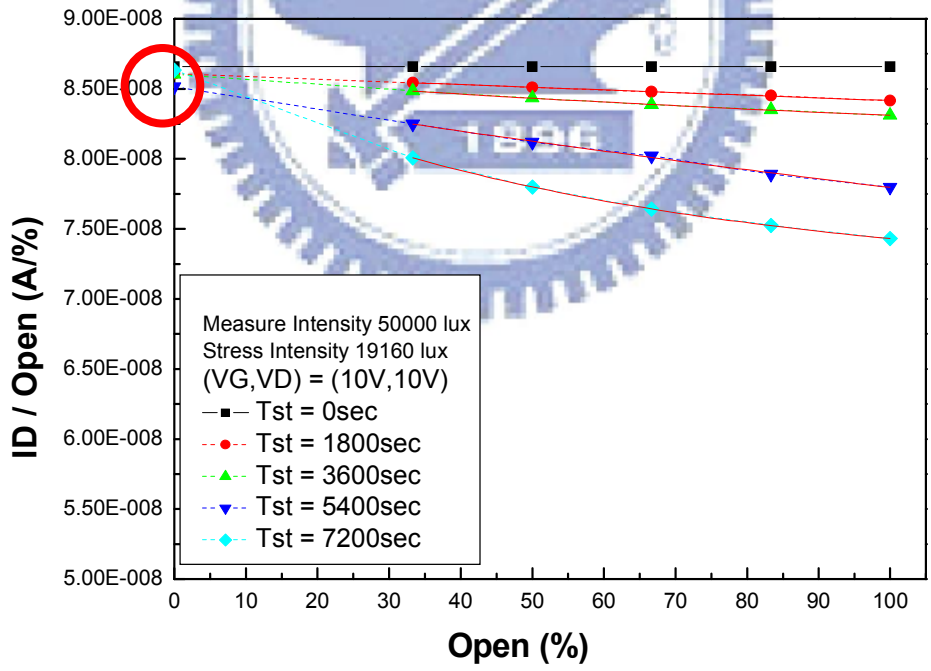

(b)

Fig. 4-16 (a) Optical stress with different light intensities and (b) I_D/Open-ratio versus open-ratio under 50000 lux illumination with different stress times and different stress light intensities

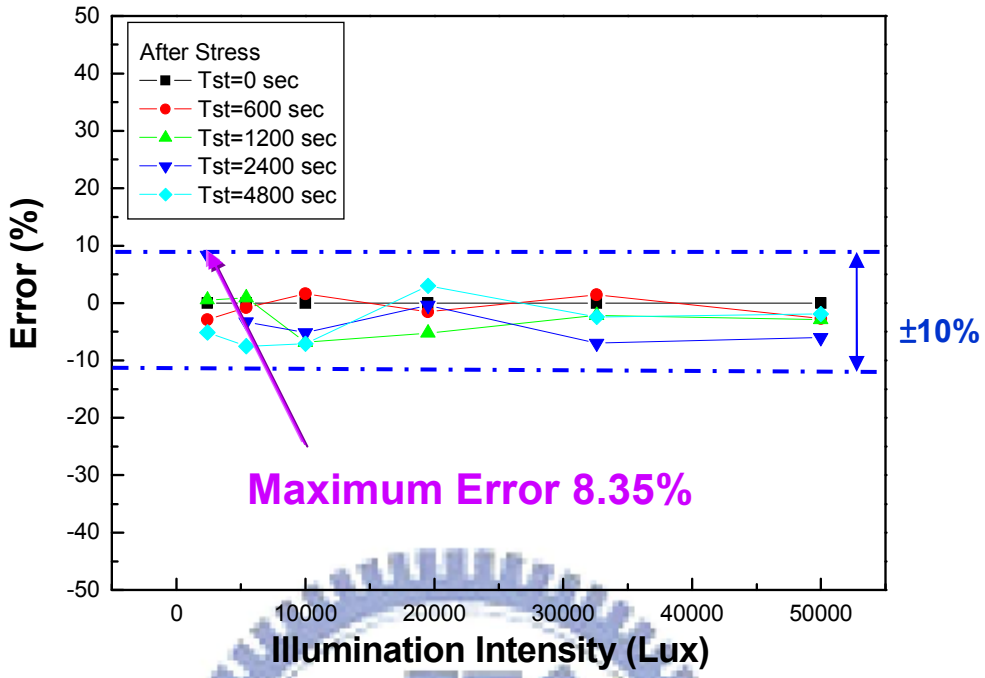

Fig. 4-16 (c) Error analysis of optical stress with different light intensities after calibration between the measured light intensity and the illuminated light intensity

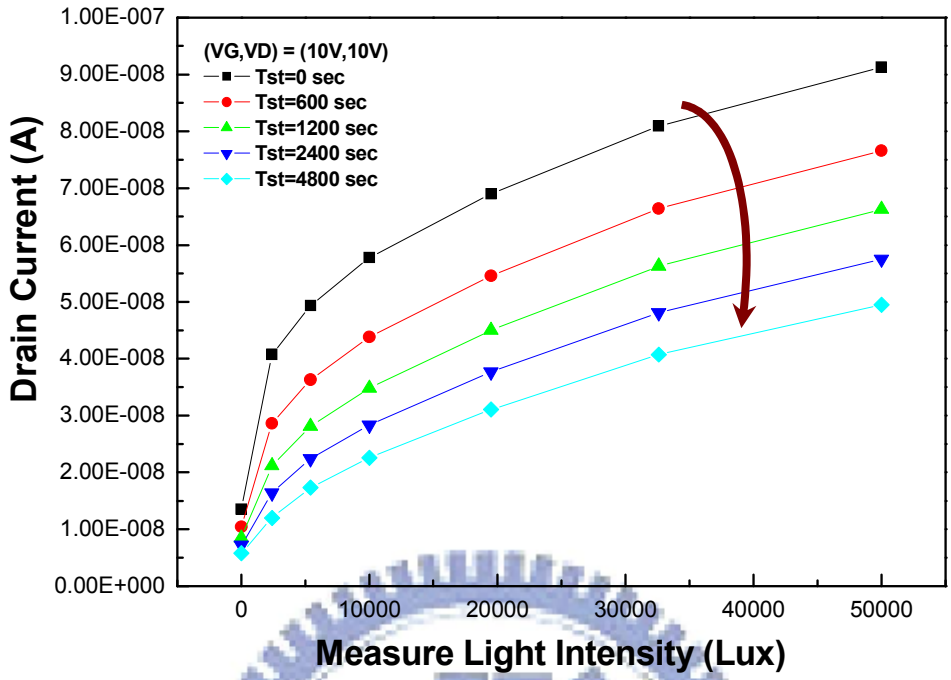

Fig. 4-17 (a) The drain current versus illumination intensity curves with different optical stress times by 19160 lux FL and 16673 lux BL at V_{DS}=10V

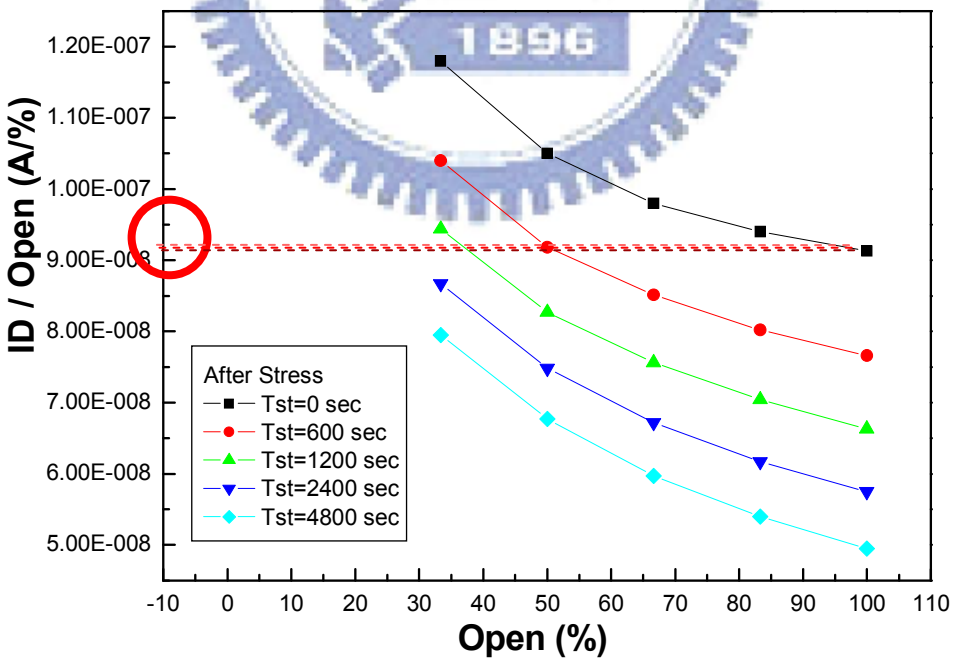

Fig. 4-17 (b) Error analysis of optical stress by 19160 lux FL and 16673 lux BL between the measured light intensity and the illuminated intensity

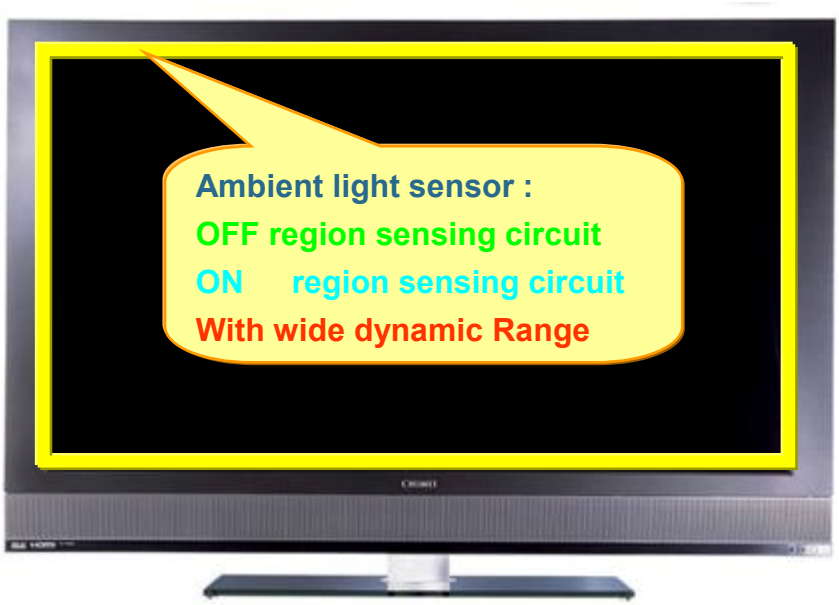

Fig. 4-18 The position of ambient light sensor in the display

Chapter 5

Conclusions

In our research, we study the application of the a-Si TFTs for light sensing with wide dynamic range. The Gap-Gate structure of a-Si:H TFT with smaller size as the sensing device is proposed to achieve high current and good photosensitivity in ON region for low illumination. In addition, we proposed the sensing circuits which can optimize the photosensitivity characteristics of the TFT in both ON and OFF regions. Moreover, we analyze the possible factors that can affect the sensing accuracy and find that SW effect is the most serious issue. We proposed a method to calibrate the error for this effect owing to the ambient light stress. However, the method is not applicable if both ambient light and backlight shine on the ambient light sensor. This sensing technique can be used in the area without backlight for example, in the peripheral area. It can provide good sensing accuracy (error < 10%) in the wide dynamic range of ambient light from 0 lux to 63315 lux.

References

[1] C.C. Lai, C.C. Tsai, “Backlight Power Reduction and Image Contrast Enhancement Using Adaptive Dimming for Global Backlight Application,” IEEE Transactions on Consumer Electronics, Vol. 54, n2, pp. 669-674, 2008

[2] Hyun-Sang Park, Tae-Jun Ha, Min-Koo Han, Doo-Hyung Woo, Kwang-Sub Shin, and Chi-Woo Kim, “A New Monolithic Polysilicon Ambient Light Sensor System with Wide Dynamic Range for Active-Matrix Displays by Employing an Adaptive Sensitivity Control Method,” SID’08 Symposium Digest, pp.716-719, 2008

[3] S. M. GadelRab, S.G. Chamberlain, “The Source-Gated Amorphous Silicon Photo-Transistor,” IEEE Transactions on Electron Devices, Vol. 44, n10, pp.1789-1794, 1997

[4] M. Hack, A. G. Lewis, R. H. Bruce, and R. Lujan, “Optically addressable input circuit for two-dimensional image sensing,” in *Proc. Mat. Res. Soc. Symp.*, vol. 219, pp. 167–172, 1991

[5] J-D. Gallezot, S. Martin, J. Kanicki, “Photosensitivity of a-Si:H TFTs,” IDW’01 Asia Display, pp.407-410, 2001

[6] W. den Boer, A. Abileah, P. Green, T. Larsson, S. Robinson, T. Nguyen, “Active Matrix LCD with Integrated Optical Touch Screen,” SID’03 Symposium Digest, pp.1494-1497, 2003

[7] A. Abileah, W. den Boer, T. Larsson, T. Baker, S. Robinson, R. Siegel, N. Fickenscher, B. Leback, T. Griffin, P. Green, “Integrated Optical Touch Panel in a 14.1” AMLCD,” SID’04 Symposium Digest, pp.1544-1547, 2004

[8] W.D. Boer, A. Abileah, P. Green, T. Larsson, “Active Matrix LCD with Integrated Optical Touch Screen,” SID’03 Tech. Digest, pp. 1494-1497, 2003

[9] B.T. Chen, Y.H. Tai, K.F. Wei, C.C. Tsai, C.Y. Huang, Y.J. Kuo, H.C. Cheng "Investigation of source-follower type analog buffer using low temperature poly-Si TFTs," Solid-State Electronics, vol. 51, pp. 354-359, 2007.

[10] S.H. Kim, E.B. Kim, H.Y. Choi, M.H. Kang, J.H. Hur, J. Jang, "A coplanar hydrogenated amorphous silicon thin-film transistor for controlling backlight brightness of liquid-crystal display," Solid-State Electronics, pp.478-481, 2007

[11] G-Y. Yang, Y-G. Kim, T-S. Kim, J-T. Kong, "S-TFT: An Analytical Model of Polysilicon Thin-Film Transistors for Circuit Simulation," IEEE Custom Integrated Circuits Conference, pp.213-316, 2000

[12] W.S. Lee, G.W. Neudeck, J. Choi, S. Luan, "A Model for the Temperature-Dependent Saturated ID-VD Characteristics of an a-Si :H Thin-Film Transistor," IEEE Transactions on Electron Devices, Vol. 38, n9, pp.2070-2074, 1991

[13] N. Tada, H. Hayashi, M. Yoshida, M. Ishikawa, T. Nakamura, T. Motai, T. Nishibe, "A Touch Panel Function Integrated LCD Using LTPS Technology," IDW'04, pp.349-350, 2004

[14] H. Hayashi, T. Nakamura, N. Tada, T. Imai, M. Yoshida, H. Nakamura, "Optical Sensor Embedded Input Display Usable under High-Ambient-Light Conditions," SID'07 Symposium Digest, pp.1105-1108, 2007

[15] M. Vanecek, A. Poruba, A. Fejfar, J. Kocka, ' Dircet measurement of the deep defect density in thin amorphous silicon films with the absolute constant photocurrent method' J.Appl. Phys., pp.6203-6210, 1995

[16] T. Kruger, 'On the origin of the Staebler-Wronski effect' J.Appl. Phys., 2006

[17] L. Eglseer, S. Horvat, H. Kroha, 'Study of the long-term behavior of the sensitivity of amorphous silicon photo detectors under illumination' ELSEVIER, 2006